

Investigating Aspartame and Acesulfame Potassium as Potential
Novel Ligands for Class A Orphan GPCRs

By

Brandon MacKinnon

A thesis submitted to the
Department of Chemistry and Biochemistry
Mount Allison University
in partial fulfillment of the requirements for the
Bachelor of Science degree with Honours
May 6, 2020

Abstract

Artificial sweeteners are gaining increasing popularity as an alternative to sugar; however, new studies in rats show that prolonged exposure to artificial sweeteners increases breast, brain, and urinary cancer risk. Concerns have been raised with the quality, safety and the long-term health risks associated with artificial sweeteners and artificial sweeteners have been shown to induce metabolic syndrome. These sweeteners have demonstrated activity that is mediated via G-protein coupled receptors (GPCRs). GPCRs mediate many of our physiological responses to stimulants; however, around 100 of these receptors are deemed orphan, and may represent targets for sweetener activation. In this study, a high throughput screening platform was used to simultaneously quantify β -arrestin recruitment to 72 orphan GPCRs. Cells expressing receptors of interest were treated with the artificial sweeteners, aspartame and acesulfame K prior to quantification of receptor activation. GPR32, GPR4, GPR12, GPR84 and MAS1 were significantly activated in response to sweetener treatment. These receptors are expressed in epithelial cells. GPR4, GPR32, and GPR84 are connected to inflammatory responses, with artificial sweeteners also causing inflammation in the body. If validated, they will represent some of the first known ligands for the orphan receptors in question and could have implications for their role in inflammatory responses.

Table of Contents

| | |
|--|----|
| Abstract | 2 |
| Acknowledgements..... | 5 |
| List of Figures | 6 |
| List of Abbreviations | 9 |
| Introduction | 10 |
| <i>G-Protein Coupled Receptors</i> | 10 |
| <i>G-Protein Coupled Receptor Cell Signalling</i> | 11 |
| <i>Human Cell Models to Study GPCR Signalling</i> | 14 |
| <i>Artificial Sweeteners as potential GPCR ligands</i> | 17 |
| <i>Aspartame</i> | 18 |
| <i>Acesulfame K</i> | 19 |
| <i>Artificial Sweeteners and GPCRs</i> | 20 |
| <i>Purpose of the Study</i> | 21 |
| Material and Methods | 21 |
| <i>Human Cell Culture</i> | 21 |
| <i>DNA Plasmid Preparation</i> | 22 |
| <i>Transfection</i> | 22 |
| <i>384-Well Plate Optimization</i> | 23 |
| <i>Screen Optimization Experiments</i> | 23 |
| <i>High-Throughput Sweetener Screens</i> | 24 |
| <i>Luciferase Assay</i> | 25 |
| <i>β- Galactosidase Assay</i> | 25 |
| <i>MTT Assay</i> | 26 |
| <i>Green Fluorescent Protein Microscopy</i> | 26 |
| <i>Data Analysis</i> | 26 |
| Results | 26 |
| <i>Optimization of High Throughput Screen</i> | 26 |
| <i>Contamination Testing</i> | 32 |
| <i>High Throughput Sweetener Screen</i> | 34 |
| Discussion | 44 |
| <i>Optimization of High Throughput Screen</i> | 44 |
| <i>Contamination Testing</i> | 44 |

| | |
|---|----|
| <i>High Throughput Sweetener Screen</i> | 45 |
| Conclusion and Future Directions | 50 |
| Literature Cited | 51 |
| Supplementary Data..... | 59 |

Acknowledgements

I would like to thank and acknowledge everyone who has in any way, shape or form been essential to the success of this project.

First and foremost, Dr. Jillian Rourke for her constant guidance and support throughout the entire process of this project. Without her patience and willingness to answer all of my questions, and there was a lot of them, this project wouldn't have worked. I couldn't have had a better supervisor and mentor for the last year and a half. Thank you for everything.

Dr. Karen Crosby for being the second reader of this thesis and for providing valuable input and feedback.

Dr. Tyson MacCormack for the use of his lab and lab equipment.

Dr. Jeffery Waller for the competent cell line, lab glassware, equipment, and expertise.

Dr. Amanda Cockshutt for lab space, equipment, and expertise.

Phil Cormier for teaching me how to properly use Liquid Nitrogen, the transportation of CO₂ tanks and answering any technical questions that I have had.

Nickolas Fernandez for helping me so much with R Studio when it was acting funny. Also, for being an amazing lab/artificial sweetener partner; couldn't have done it without you.

Rachel McDougall for help with lab work and for being an amazing lab mate and friend. Would not have been able to get through the last four years without you.

Madeline Power for being a wonderful lab partner but an even better friend and person. It's been a crazy two and a half years! Thank you for everything you've done!

Madelaine Russel for autoclaving almost everything at any given time and for being a great lab partner. Thank you.

Tyler Lutes from Sorcimmed for the use of the EVOS microscope and the answering of any and every question we had.

Pat Gormley for teaching me how to safely operate the autoclave.

My friends I've made here at Mount Allison, thank you for being a part of my story and allowing me to talk about GPCRs all the time, especially my roommate Jordan; couldn't have done it without you, buddy. Also, thanks 20 Park St. for that lesson on aspartame.

To my parents and sister, I am beyond grateful for you, none of this would even be possible without your encouragement, unconditional love, and support. I've been hard to deal with at times throughout this entire process and I am forever grateful for the sacrifices you all have made. From the bottom of my heart thank you.

Lastly, thank you to NBIF for funding this project and to Mount Allison University for providing me with this amazing opportunity and teaching me more than just biochemistry these last four years.

List of Figures

Figure 1: Secondary structure and location of agonist binding for different GPCRs. Showing the alternating hydrophobic transmembrane α -helical segments. Image taken from Kobilka, 2007.

Figure 2: The GPCR cycle which starts with a GPCR in its basal state and progresses through the conformational changes and phosphorylation events that must occur to return to a basal state after a ligand has bound to the receptor. Image taken from Hanlon and Andrew, 2015.

Figure 3: Modular design of TANGO expression constructs (top). General scheme for β -arrestin recruitment Tango or PRESTO-Tango (bottom). Components of the Tango system serve the following functions: The HA signal (hemagglutinin tag) promotes membrane localization N-terminal FLAG epitope to monitor GPCR membrane expression, the GPCR gene, vasopressin receptor (V_2 tail) promotes arrestin recruitment, TEV-beta arrestin fusion cleaves at the TEV cleavage site, and a tetracycline transactivator (tTA) transcription factor required for luciferase expression in response to receptor activation. Image taken from Kroeze *et al.* 2015.

Figure 4: PRESTO-TANGO 384-well format. Image taken from Kroeze *et al.* 2015.

Figure 5: Aspartame (**A**) and Acesulfame potassium (**B**) chemical structure. Created with ChemDraw Software.

Figure 6: Plate layout for the HTS of artificial sweeteners with the orphan receptors being placed in wells labeled R1-R8 and the controls of green fluorescent protein (GFP), pBluescript II SK+ (pBSK, NT) and Lysophosphatidic Acid Receptor 1 (LPAR1) being placed on the sides.

Figure 7: The optimization of lysate sample and luciferin working solution using a BioTek plate reader to measure LPAR1 (**A**) and LPAR2 (**B**) luminescence and a SpectraMax reader to measure LPAR1 (**C**) and LPAR2 (**D**) luminescence via a vehicle, 10% FBS and 20% FBS samples. Treatment ratios of lysate sample, water and working solution in μL are as follows: A – 10:10:10, B – 10:5:15, C – 10:0:20, D – 5:15:10, E – 5:10:15, F – 5:5:20. Data are shown as mean \pm SEM, where N=3.

Figure 8: Determination of optimal positive control receptor and treatment conditions for PRESTO-Tango screen protocol (**A**) and fold change (**B**), and LPAR2 RLU values (**C**) and fold change (**D**). The graph is plotted with the treatments of the receptor against the RLU of each receptor found by a Luciferase assay and β -Gal assay. Data are shown as mean \pm SEM, where N=3.

Figure 9: The optimization of PEI reagent using a β -Gal Assay (Absorbance at 420 nm) at four-time intervals; 5 minutes (**A**), 10 minutes (**B**), 20 minutes (**C**) and 30 minutes (**D**) against six different amounts of PEI that were added to each well. 0.3 μL was determined to have the largest absorbance in all four-time intervals. Data are shown as mean \pm SEM, where N=3.

Figure 10: The GFP transfection efficiency percentage is based on the amount of PEI and how well it transfected the GFP plasmid (**A**) into the HTLA Cells (**B**). It was determined that 0.3 μL of PEI had the best GFP transfection percentage in comparison to the other amounts (**C**). Data are shown as mean \pm SEM, where N=3.

Figure 11: PEI optimization with varying amounts of HTLA cells plated per well. It was concluded that keeping the cells plated at or below 20 000 cells per well leads to the least amount of variability between sets (**A**). Wells with 0.3 μ L PEI leads to the greatest percentage of GFP transfection with $27.1 \pm 1.3\%$ (**B**). Data are shown as mean \pm SEM, where N=3.

Figure 12: Contamination testing revealed that there was no mycoplasma within the HTLA cell line (**A**). Running the PEI contamination test found that apoptotic bodies formed from the PEI after 24 hours of transfection (**B**). When completely optimized the normal HTLA cells (**C**) should yield high transfection efficiency shown by GFP (**D**).

Figure 13: The LPAR1 controls of the HTS that show the RLU and fold changes per plate that are used to compare to potential orphan receptor hits. Orphan screen Set A RLU (**A**) and fold change (**B**), orphan screen Set C RLU (**C**) and fold change (**D**), orphan screen Set D RLU (**E**) and fold change (**F**), and orphan screen Set E RLU (**G**) and fold change (**H**). Data are shown as mean \pm SEM, where N=3.

Figure 14: A heatmap diagram of orphan receptors treated with an aspartame and acesulfame potassium mixture. The significance level (p-value) is of the change in luminescent signaling between the NNS treatments and Opti-MEM control for the 72 orphan receptors. The four biological replicates are signified as A, C, D and E. R7 (GPR12), R37 (GPR32), R42 (GPR4), R53 (GPR84) and R58 (MAS1) are highlighted in red, as they were deemed to have a significant change in luminescence.

Figure 15: RLU (**A**) and fold change (**B**) for GPR32 when treated with 3X artificial sweetener mixture containing aspartame and acesulfame potassium relative to the vehicle treatment. Shapiro test, Bartlett's test, T-test, and Mann-Whitney U test showed that there was significance ($p < 0.05$) between sweetener and control treatments as shown with an asterisk (*). Data are shown as mean \pm SEM, where N=3.

Figure 16: RLU (**A**) and fold change (**B**) for GPR12 when treated with 3X artificial sweetener mixture containing aspartame and acesulfame potassium relative to the vehicle treatment. Shapiro test, Bartlett's test, T-test, and Mann-Whitney U test showed that there was significance ($p < 0.05$) between sweetener and control treatments as shown with an asterisk (*). Data are shown as mean \pm SEM, where N=3.

Figure 17: RLU (**A**) and fold change (**B**) for GPR4 when treated with 3X artificial sweetener mixture containing aspartame and acesulfame potassium relative to the vehicle treatment. Shapiro test, Bartlett's test, T-test, and Mann-Whitney U test showed that there was significance ($p < 0.05$) between sweetener and control treatments as shown with an asterisk (*). Data are shown as mean \pm SEM, where N=3.

Figure 18: RLU (**A**) and fold change (**B**) for GPR84 when treated with 3X artificial sweetener mixture containing aspartame and acesulfame potassium relative to the vehicle treatment. Shapiro test, Bartlett's test, T-test, and Mann-Whitney U test showed that there was significance ($p < 0.05$) between sweetener and control treatments as shown with an asterisk (*). Data are shown as mean \pm SEM, where N=3.

Figure 19: RLU (A) and fold change (B) for MAS1 when treated with 3X artificial sweetener mixture containing aspartame and acesulfame potassium relative to the vehicle treatment. Shapiro test, Bartlett's test, T-test, and Mann-Whitney U test showed that there was significance ($p < 0.05$) between sweetener and control treatments as shown with an asterisk (*). Data are shown as mean \pm SEM, where N=3.

Figure 20: The transfection efficiency of GFP using various concentrations of PEI in each cell well at various plated cell per well amounts; 5000 (A), 10 000 (B), 15 000 (C), 20 000 (D), 25 000 (E) and 30 000 (F) cells per well.

Table 1: GPCR screen receptor number and the corresponding official GPCR orphan receptor name along with RLU value and P-Value determined using R Studio, where N=3.

Table 2: GPCR receptor and the corresponding Rourke lab stock number, concentration (ng/ μ L) as well as the A260/A280 ratio. Prepped using the Promega Pure Yield Miniprep and concentrations were found using the Nanodrop software.

Table 3: PEI transfection efficiency calculated by GFP cells counted at 10X magnification using an EVOS microscope versus the total number of cells counted at 10X magnification.

List of Abbreviations

| | |
|--------------|--|
| Ace K | Acesulfame Potassium |
| Acesulfame K | Acesulfame Potassium |
| DAPI | 4',6-Diamidino-2-Phenylindole |
| DMEM | Dulbecco's Modified Eagle's Medium |
| DNA | Deoxyribonucleic Acid |
| FBS | Fetal Bovine Serum |
| GDP | Guanosine Diphosphate |
| GFP | Green Fluorescent Protein |
| GPCR | G-Protein Coupled Receptor |
| GRKs | G Protein-Coupled Receptor Kinases |
| GTP | Guanosine Triphosphate |
| HEK293/ HTLA | Human Embryonic Kidney Cells |
| HTS | High Throughput Screen |
| IsoP | Isoproterenol |
| JNK3 | c-Jun N-Terminal Kinase 3 |
| LB | Lysogeny Broth |
| LPA | Lysophosphatidic Acid |
| MTT | 3-(4,5-Dimethylthiazol-2-Yl)-2,5-Diphenyltetrazolium Bromide |
| NNS | Non-Nutrient Sweetener |
| P/S | Penicillin - Streptomycin |
| PBS | Phosphate Buffered Saline |
| pBSK | pBluescript SK |
| PEI | Polyethylenimine |
| PRESTO-Tango | Parallel Receptor-ome Expression and Screen via Transcriptional Output - TANGO |
| RLU | Luminscene/Absorbance 420 |
| SEM | Standard Error of the Mean |
| TEV | Tobacco Etch Virus |
| tTA | Tetracyclin Transactivator |
| β -Gal | β -Galactosidase |

Introduction

G-Protein Coupled Receptors

G-protein-coupled receptors (GPCRs) mediate the majority of our physiological responses to stimulants like hormones and neurotransmitters. GPCRs have become a major target for therapeutic techniques and over the past three decades, great progress has been made with understanding the structure and function of GPCRs. GPCRs are the largest family of membrane proteins that have many functions including being responsible for vision, taste, and olfaction. All GPCRs are characterized by the presence of seven hydrophobic transmembrane α -helical segments separated by alternating intracellular and extracellular loops, as shown in Figure 1 (Rosenbaum *et al.* 2009). GPCRs share the most homology within these transmembrane

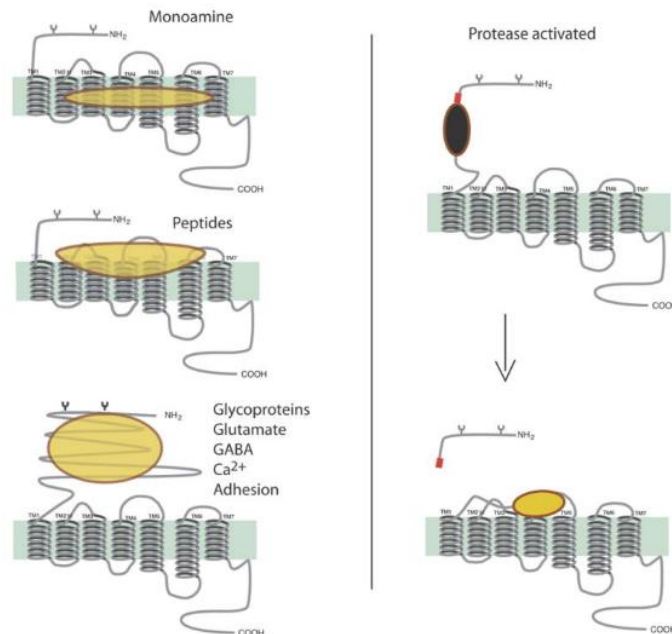


Figure 1: Secondary structure and location of agonist binding for different GPCRs. Showing the alternating hydrophobic transmembrane α -helical segments. Image taken from Kobilka, 2007.

segments while the most variable structures in the GPCRs are at the carboxyl terminus, an intracellular loop that spans the fifth and sixth transmembrane, and the amino terminus (Kobilka, 2006). A detailed analysis of the human genome revealed over 800 unique GPCRs that were further classified into five families at the time; the rhodopsin family (Class A, 701 members), the

secretin family (Class B, 15 members), the glutamate family (Class C, 15 members), the adhesion family (24 members) and the frizzled/taste family (24 members) (Frekrissson *et al.* 2003). The Class B family has been reassigned to the adhesion family creating four families for classification instead of five (Alexander *et al.* 2017).

An orphan GPCR receptor is defined as having unknown physiological function and/or endogenous ligand. Of the 800 GPCRs, there are 121 orphan receptors (Alexander *et al.* 2017). Deorphanization of GPCRs is ongoing as they are a promising group of pharmaceutical targets, so the orphan list is continuing to go down (Kobilka, 2007). The Class A GPCRs are the most widely investigated drug targets for pharmaceutical companies. The class A GPCRs can have multiple interacting partners with ligands, allosteric modulators, and signalling proteins which make them ideal for therapeutic companies (Cong *et al.* 2017). Rhodopsin is the founding member of the Class A GPCR family and its crystal structure was solved in 2000 which has allowed for several function states to also be solved (Xu and Xiao, 2012). Despite extensive research, 87 Class A GPCRs are still classified as orphan receptors (Alexander *et al.* 2017).

G-Protein Coupled Receptor Cell Signalling

GPCR signalling has been a focus for researchers for several decades. Leading to many discoveries of therapeutic techniques, as well classifying orphan receptors based on their ligands; one of which is Rhodopsin. Rhodopsin, the prototypical class A GPCR, was the first identified to have activation that involved rigid body motion of the α -helices (Gurevich and Gurevich, 2017). This motion then resulted in the cytoplasmic side of the membrane opening a cavity. GPCRs can never have their conformational equilibrium shifted to a single active or inactive state thus different proteins that interact with the GPCRs (ligands) must prefer selective conformations.

Localization of a GPCR on the cell membrane can affect the ability it has to signal, with lateral movement often being restricted by preferential localization of GPCRs to specific lipid environments (Allen *et al.* 2007). The ligand-receptor binding event must be responded to by the cell itself using the effectors of the GPCR. Once a heterotrimeric complex comes into contact with a ligand-GPCR receptor, downstream signalling starts, and conformational changes begin. Each G_{α} protein targets a specific signalling cascade and depending on which G_{α} protein the GPCR encounters, a different response/cascade is initiated (Hanlon and Andrew, 2015).

As GPCRs are the receptors for hormones, neurotransmitters, ions, photons, and other stimulants, their signal transduction plays critical roles in intercellular communication in vertebrate physiology. Classically, an agonist would bind with the GPCR to activate the specific heterotrimeric G proteins which cause activation of an effector protein cascade (Figure 2). The heterotrimers activate different signalling pathways; the G_{α} proteins, which are GTPases, catalyzes the hydrolysis of the two states GTP bound to GDP bound, where the GTP bound state is the active state (Volger *et al.* 2008). The G_{β} is tightly linked to the G_{γ} subunit through hydrophobic interactions (Higgins and Caseys, 1994) and the G_{γ} protein is prenylated at the C-terminus to promote membrane localization (Sondek *et al.* 1996).

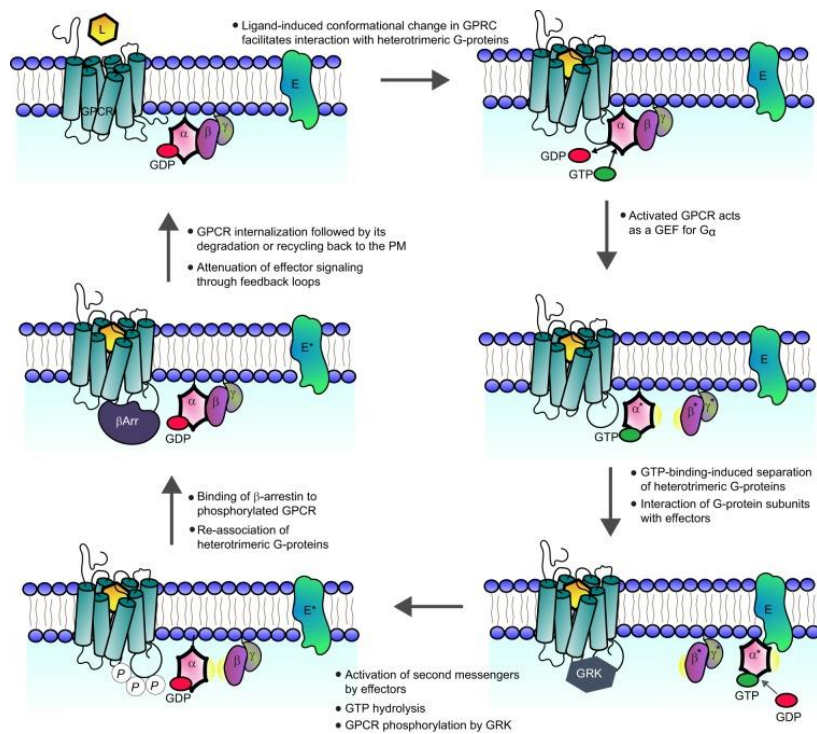


Figure 2: The GPCR cycle which starts with a GPCR in its basal state and progresses through the conformational changes and phosphorylation events that must occur to return to a basal state after a ligand has bound to the receptor. Image taken from Hanlon and Andrew, 2015.

GPCRs have multiple signal transducers; G-proteins, GRKs and arrestins. There are four arrestin proteins in mammalian species that regulate the signaling and trafficking of G-protein-coupled receptors. Arrestin 1 and 4 are associated with signalling in retinal rods and cones and are subsequently known as visual arrestins. Arrestin 2 and 3 are known as β -arrestins and are used in the function of signal transduction of non-visual receptors (Gurevich and Gurevich, 2006). β -arrestin-2 activates the JNK3 cascade, but it does not depend on the ability to bind receptors. β -arrestin-1 is a part of the core mechanism of programmed cell death (Gurevich and Gurevich, 2017).

In addition to the classical heterotrimeric G protein activation, GPCRs can have a more complex signalling behaviour including simultaneous activation of multiple pathways, phosphorylation events, and arrestin-mediated internalization, all of which shape the overall

response. GPCR activity is further diversified by oligomerization creating opportunities for responses localized to a specific membrane compartment and by different ligands binding to the same receptor (Rosenbaum *et al.* 2009).

Ligands can be grouped into different efficacy classes based on their ability to elicit a response from the receptor. The classes are defined by full agonist, which is capable of maximal receptor stimulation; partial agonist, which cannot elicit a full response but does cause some activity of the receptor; neutral antagonist which has no effect on activity of a receptor but it can stop other ligands from binding to the receptor; and finally inverse agonist, which reduces the basal activity of the unliganded receptor (Rosenbaum *et al.* 2009). Ligand efficacy is described by energy transfer between the binding pocket and the G-protein interaction site; this action is dependent on multiple interactions between receptor and agonist (Weis and Kobilka, 2018). It was found that GPCR activation has distinct conformations that are stabilized by ligands which achieve varying efficacies for different signalling pathways that can interact with specific effectors (Rosenbaum *et al.* 2009).

Human Cell Models to Study GPCR Signalling

GPCR signalling is needed to help progress therapeutic companies to create new and improving drugs. As we learn more on how GPCRs signal we slowly learn how important they are for our physiological function; however, there are numerous challenges associated with studying GPCR signalling, including the condition of the cells and if the correct ligand can be found. Western blots and biochemical assays are done for intracellular mediators; however, these have limitations with orphan receptors because there are no known comparisons when working with these receptors.

Human Embryonic Kidney (HEK) 293 cell lines are widely used in biology and biochemistry to study signal transduction, protein interactions, small scale protein expression and more. The original cell line was derived in 1973 when the kidney of an unknown aborted embryo was transformed with adenovirus 5 DNA (Lin *et al.* 2014). The HEK 293 cells that were worked with in this study are HEK 293 HTLA cells that were stably transfected with the β -arrestin-TEV protease and the tTA dependent reporter gene that allows the PRESTO-Tango assay to work.

In response to the growing need for research tools to measure cell surface receptor activation, Barnea *et al.* (2008) developed an experimental strategy to monitor the protein interactions in a cell with high selectivity (Figure 3). The Barnea technique uses a transcription factor that binds to a receptor containing a linker which has a cleavage site for a protease. The activation of the receptor then recruits a signalling protein attached to a protease that cleaves the site and causes the transcription factor to activate the gene. The assay relies on introducing exogenous genes into the cell including the transcription factor-modified receptor, the protease modified- effector protein, and a transcription factor-dependent luciferase reporter gene. They called this assay a Tango assay due to it relying on two proteins to stimulate a response. The Tango assay for GPCRs monitored the activation of a receptor by a ligand by the ligand-mediated arrestin binding. Almost all GPCRs accompany arrestin upon activation, so they used this knowledge of arrestin recruitment to develop an assay that included all known GPCR classes. The Tango assay sensitivity and the ability to monitor a receptor without interference has allowed for GPCR orphans to be studied. Which in the paper by Barnea *et al* (2008) they found that GPR1 is activated by chemerin which was confirmed by an independent Ca^{2+} mobilization assay.

To facilitate the study of multiple receptors in this way, Kroeze *et al.* 2015 adapted the original method for β -arrestin recruitment which they called PRESTO-TANGO, meaning Parallel Receptorome Expression and Screening via Transcriptional Output – TANGO, for the simultaneous and parallel interrogation of the entire GPCR-ome. The underlying principle of the adaptation was to make the GPCR in a way that modules could be excluded or included by having a cleavable signal sequence (HA Signal) at the 5' end to promote membrane localization as well as a FLAG epitope to monitor cell expression. At the 3' end there is a TEV cleavage site and a tetracycline transactivator, as well as a C-terminal fragment from the human vasopressin receptor, which is a short amino acid sequence added to promote sustained arrestin recruitment.

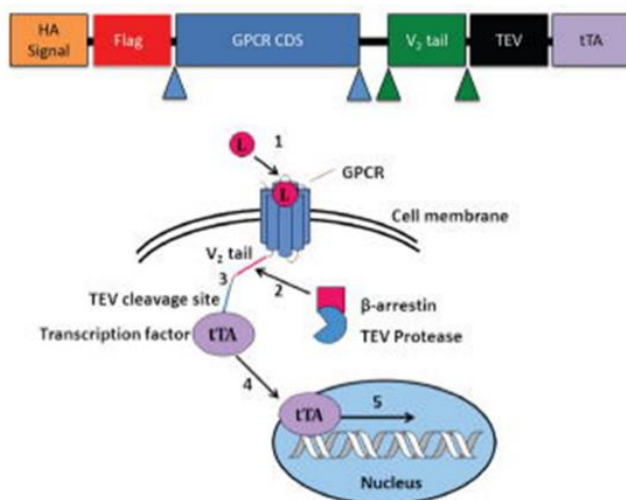


Figure 3: Modular design of TANGO expression constructs (top). General scheme for β -arrestin recruitment Tango or PRESTO-Tango (bottom). Components of the Tango system serve the following functions: The HA signal (hemagglutinin tag) promotes membrane localization N-terminal FLAG epitope to monitor GPCR membrane expression, the GPCR gene, vasopressin receptor (V₂ tail) promotes arrestin recruitment, TEV-beta arrestin fusion cleaves at the TEV cleavage site, and a tetracycline transactivator (tTA) transcription factor required for luciferase expression in response to receptor activation. Image taken from Kroeze *et al.* 2015.

The PRESTO-TANGO screening allowed a 384-well plate design to simultaneously test multiple receptors and treatments where luminescence was measured as an indicator of receptor activation. Using this high-throughput adaptation, Kroeze *et al* identified new drug ligands for

the MRGPRX receptor and established the PRESTO-TANGO methodology as a powerful high throughput tool for deorphanizing GPCRs (Kroeze *et al.* 2015).

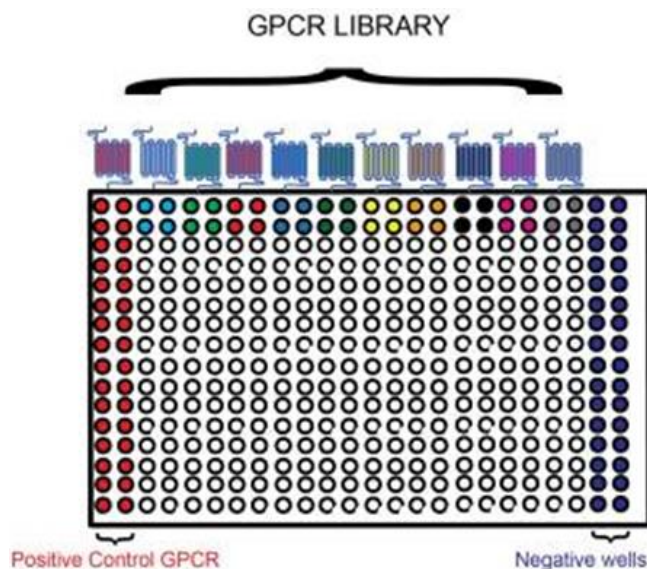


Figure 4: PRESTO-TANGO 384-well format. Image taken from Kroeze *et al.* 2015.

Artificial Sweeteners as potential GPCR ligands

Artificial sweeteners are increasing in popularity as an alternative to sugar with an increase in obesity, diabetes, and metabolic syndrome. The shift to low-calorie artificial sweeteners has amplified in today's society. The artificial sweeteners are also called non-nutritive sweeteners (NNS) which provide more intense sweetness with little to no calories. Aspartame and acesulfame potassium have been labeled as safe by the United States Food and Drug Administration (US-FDA) (Sharma *et al.* 2016). New data from both humans and non-human animals have shown evidence that NNS play an active role in the gastrointestinal tract as well as trigger a response in T1R and α -gustducin taste receptors. A study showed that in mice, the stimulation of intestinal taste receptors by sucralose led to the more expeditious absorption of sugars into the bloodstream (Brown *et al.* 2010). It was concluded that consumption of artificial

sweeteners with sugar containing food/drink could lead to increases in sugar absorption and insulin secretion.

Concerns have been raised with the quality, safety and the long-term health risks associated with artificial sweeteners. Artificial sweeteners have been shown to induce metabolic syndrome but the mechanism by which they dysregulate the host metabolism remains unknown. What is known is that the sweeteners often disrupt the growth of gut bacteria but the specific effects on gut microbiota remains largely undiscovered (Bian *et al.* 2017). Heavy artificial sweetener use consisting of a combination of acesulfame K and aspartame over an extended period of time causes urinary tract tumors (van Eyk, 2015). Aspartame has also been linked to malignant tumors for breast and brain cancer in rats. Tests done with human cancer cells and artificial sweeteners showed that there were morphological alterations of the test cells when the sweeteners were added in concentrations greater than 10 mM (van Eyk, 2015).

Aspartame

Aspartame was the third sweetener discovered and it is approximately 200 times sweeter than table sugar. Aspartame consists of two amino acids (Figure 5A): aspartate and phenylalanine (van Eyk, 2015). Aspartame is hydrolyzed in the intestines into phenylalanine (50%), aspartic acid (40%) and methanol (10%) during metabolism in the body. Aspartame is metabolized by hydrolysis of the methyl group by intestinal esterases which yield methanol which in turn is often oxidized to CO₂. The dipeptide is split by dipeptidase and the free amino acids are absorbed. Aspartic acid is transformed to CO₂ through the tricarboxylic acid cycle. Phenylalanine is absorbed into body protein either unchanged or as its major metabolite, tyrosine (Ranney *et al.* 1976). It is possible for metabolites to act as chemical signals and bind and activate GPCRs (Husted *et al.* 2017 and Hooper *et al.* 1994).

It has been found that the aspartame metabolites have negative effects in the body; excess phenylalanine blocks amino acid transport to the brain which causes a decrease in dopamine and serotonin production (Pietz *et al.* 1999). Aspartic acid in high concentrations causes hyperexcitability of neurons; the excess of aspartic acid and the lack of astrocytic uptake induces excitotoxicity that leads to the degradation of neurons as well as astrocytes. The methanol metabolite has the ability to cause central nervous system depression, vision disorder, and other complications that lead to metabolic acidosis or coma (Rycerz and Jaworska-Adamu, 2013). Choudhary and Lee, 2018 concluded that aspartame may be responsible for adverse neurobehavioral health outcomes and that the consumption of aspartame needs to be done cautiously.

Acesulfame K

Acesulfame K (Figure 5B) is also approximately 200 times sweeter than table sugar; however, unlike aspartame after ingestion acesulfame K is not metabolized and is excreted unchanged in the urine (van Eyk, 2015). Acesulfame K has been found to be genotoxic and can cause inhibition of glucose fermentation in intestinal bacteria. Acesulfame K is a sulfonamide which is a chemical that is associated with antimicrobial activity. Acesulfame K is believed to increase the potential of developing chronic inflammation in the intestines and gut by disrupting the associated pathways, as well as disrupting the gut bacteria (Bian *et al.* 2017). A study on mice determined that there was a loss of cognitive function after long term use of a low carbohydrate and acesulfame K diet which caused a decrease in short term and object memories in a Y-maze and object recognition (Ibi *et al.* 2018).

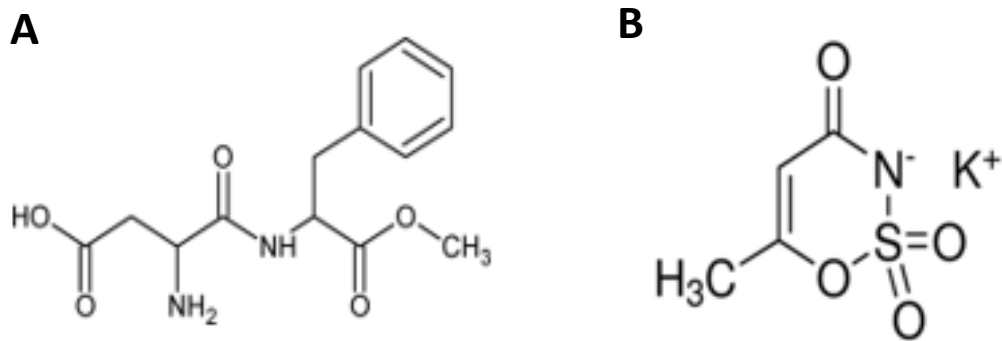


Figure 5: Aspartame (A) and Acesulfame potassium (B) chemical structure. Created with ChemDraw Software.

Artificial Sweeteners and GPCRs

The sweet taste receptor is believed to be a heterodimer of the Class C GPCRs T1R2 and T1R3. Sugars and artificial sweeteners like saccharin and acesulfame potassium bind primarily to T1R2 with some studies showing that they can bind to T1R3 (Simon *et al.* 2013). It has been shown that sweet taste receptors are activated in response to artificial sweeteners; however, some knock-out studies suggest other receptors have the capacity of binding artificial sweeteners (Simon *et al.* 2013). It has been shown that two water molecules could play an important role in sweetener binding by forming hydrogen bridges between the receptors (T1R2 and T1R3) and the sweetener ligand. The artificial sweetener aspartame had key binding residues and interacted with salt bridges, hydrogen bonds and hydrophobic interactions (Maillet *et al.* 2015).

Purpose of the Study

Based on this knowledge of artificial sweeteners and their key roles within the body, the purpose of the study that it is to conduct preliminary trials to determine if artificial sweeteners, aspartame or acesulfame potassium are ligands for some of the 72 Class A orphan receptors using the PRESTO-Tango technique for high throughput screening. Another goal of this study was to optimize the high throughput screen, so that the preliminary data would be consistent through each set of the screen.

Material and Methods

Human Cell Culture

All cells are modified Human Kidney Cells (HTLA Cells) containing the required genes for the Tango assay (luciferase, beta-arrestin fusion) unless otherwise stated. Normal growth conditions for the HTLA cells was incubation at 37°C in Complete Dulbecco's Modified Eagle Media (Wisent Bioproducts, 319-005-CL) with 10% Fetal Bovine Serum (FBS) and passaging every two to four days. Passaging the HTLA cells involved removing the media, followed by a wash with either PBS or serum-free DMEM. Then, 2.5% trypsin was placed on the cells and incubated for 2 minutes at 37°C. Cells were resuspended in DMEM before centrifugation for 5 minutes at 300 times gravity. Cells were resuspended in serum-free DMEM then seeded in a 10 cm² cell culture plate with complete DMEM. 100 µg/mL Hygromycin B and 2 µg/mL puromycin was also added to the seeded plate.

To plate the HTLA cells for an experiment, sub-culturing was carried out by a wash with serum-free DMEM from Multicell, followed by incubation with 2.5% trypsin for 2 minutes at

37°C. Cells were resuspended in complete DMEM before centrifugation for 5 minutes at 300 times gravity. Cells were resuspended in serum-free DMEM. A one in one mixture of cells and trypan blue was combined in a 1.5 mL Eppendorf tube. The mixture was placed on a hemocytometer and the cells were counted to determine the desired cell concentration of 20,000 cells per well for the experiment. The cells were then plated in a 96-well plate(s) in 1% serum. The 96-well plate(s) were then incubated for 24 hours at 37°C.

DNA Plasmid Preparation

LB agar plates containing 50 µg/mL ampicillin were warmed to 37°C. Frozen PRESTO-TANGO GPCR expression vector glycerol stocks in *E.coli* were scraped with a pipet tip and streaked across the LB agar plate. Once all receptors were streaked, the plates were inverted and placed in 37°C incubation for 18 hours. Following the incubation, a single isolated colony was picked with a pipet tip and inoculated in LB broth containing 50 µg/mL ampicillin. The LB broth was incubated for 18 hours at 37°C with 250 rpm oscillation. A 25% glycerol stock was made with LB culture. Miniprep was done following Machery Nagel NucleoSpin Transfection grade kits. Nanodrop technology was used to determine the 260/280 ratio as well as the concentration of the sample.

Transfection

Transfection mixture was made up using 25 ng pCMV-βal, 50 ng pBSK, 25 ng PRESTO-TANGO plasmid (Roth Lab), 0.2 µg of polyethylenimine (PEI), and Opti-MEM. Transfection mix replaced cell medium and was incubated for 24 hours at 37°C. Media was removed and replaced with 3X treatments prepared in Opti-MEM for a final concentration of 10% FBS and 20% FBS and incubated for 24 hours at 37°C. Cell media was removed, and cells were lysed with 1X Reporter Lysis Buffer, rocked for 15 min, then froze at -80°C.

384-Well Plate Optimization

Luciferase assay buffer was prepared using D-luciferin (Biotium, 30028-L2) and luciferase buffer. Six samples of lysate from HTLA cells were transfected with either DNA for the positive control GPCRs Lysophosphatidic Acid Receptor 1 (LPAR1) or LPAR2 and treated with vehicle, 10% FBS or 20% FBS mixed with varying amounts of water and buffer solutions. Each treatment of sample, water and buffer was added to a 384 well plate and luminescence was measured on a SpectraMax reader and a BioTek Multimode Microplate Reader.

Screen Optimization Experiments

There were more optimization experiments done which followed the *Human Cell Culture* procedure outlined above with the follow variations: transfection optimization of LPAR1 and LPAR2 differed with the transfection mixture being made up using 25 ng pCMV- β gal, 50 ng pBSK, 25 ng PRESTO-TANGO plasmid (LPAR 1, LPAR 2 and GFP).

The two PEI optimization experiments varied by using varying concentrations of PEI which included 0.05, 0.1, 0.2, 0.3, and 0.4 μ g for the first one. The second test, in sets of 16 wells, cells were plated at the concentrations of 5 000, 10 000, 15 000, 20 000, 25 000 and 30 000 cells per well. The varying concentrations (0.1, 0.2, 0.3, and 0.4 μ g) of PEI were used for this experiment. GFP transfection efficiency was determined by manual counting.

The first contamination test used HTLA and HEK cells from -80°C and liquid nitrogen storage and were cultured for the duration of this experiment in high glucose (4.5 g/L) DMEM media supplemented with 10% FBS. Cells were plated at 5,000 cells per well in 1% serum. All media was then removed from each well after treatment and replaced with 1 in 5000 Hoechst 33342 dye in PBS. It was incubated for 5 minutes at room temperature and washed three times with PBS having the last remain in the well. The wells were then measured via fluorescence

microscopy using the DAPI function on the EVOS microscope to determine if contamination was present at the cellular level.

The second contamination test plated the cells at 25,000 cells per well in 1% serum. The transfection mixes included 48 wells with DNA and PEI and 48 wells with just PEI. 24 wells of each set contained old PEI and 24 wells of each set contained newer PEI. Transfection mix replaced cell medium and was incubated for 6, 18 and 24 hours at 37°C. Media was removed and replaced with 3X treatments prepared in Opti-MEM and Complete DMEM with 48 wells getting Opti-MEM and 48 Wells getting DMEM. GFP was monitored at 18, 24 and 48 hours post transfection. An MTT assay was then completed to determine cell death based on the conditions stipulated.

High-Throughput Sweetener Screens

Before starting the High Throughput Screen (HTS), the 72 receptors were all prepared in a 96 well plate at 5 ng/uL so that there was enough for 3 full screens. The same was done with the β -Gal, pBSK, GFP and PEI. Treatments of sweeteners were prepared at 30X so they could be diluted to 3X on treatment day. 6 plates of HTLA cells at 60% confluence were harvested for the duration of this experiment in high glucose (4.5 g/L) DMEM media supplemented with 10% FBS. Sub-culturing was done following the method explained above in *Human Cell Culture* section. Nine 96-well plates were plated at 20,000 cells per well in 1% serum. The 96-well plates were incubated for 24 hours at 37°C. Transfection mixture was made up using 25 ng pCMV- β gal, 50 ng pBSK, 25 ng PRESTO-TANGO plasmids (72 orphan receptors with 8 receptors on each plate, along with GFP, pBSK and LPAR1 controls), 0.2 μ g of PEI, and Opti-MEM (Figure 6). Transfection mix replaced cell medium and was incubated for 12-18 hours at 37°C. Media was removed and replaced with 3X treatments of Opti-MEM and 3X sweetener mix incubated for 12-

18 hours at 37°C. GFP transfection efficiency was monitored, cell media was removed, and cells were lysed with 1X Reporter Lysis Buffer, rocked for 15 min, then froze at -80°C. Luciferase and β -Gal Assays were then completed, and data analysed following the procedure listed below.

| | 1 | 2 | 3 | 4 | 5 | 6 | 7 | 8 | 9 | 10 | 11 | 12 |
|---|---|-----|----|----|----|----|----|----|----|----|----------|----|
| A | | | | | | | | | | | | |
| B | | GFP | R1 | R2 | R3 | R4 | R5 | R6 | R7 | R8 | LPAR (-) | |
| C | | NT | R1 | R2 | R3 | R4 | R5 | R6 | R7 | R8 | LPAR (-) | |
| D | | NT | R1 | R2 | R3 | R4 | R5 | R6 | R7 | R8 | LPAR (-) | |
| E | | NT | R1 | R2 | R3 | R4 | R5 | R6 | R7 | R8 | LPAR (+) | |
| F | | GFP | R1 | R2 | R3 | R4 | R5 | R6 | R7 | R8 | LPAR (+) | |
| G | | GFP | R1 | R2 | R3 | R4 | R5 | R6 | R7 | R8 | LPAR (+) | |
| H | | | | | | | | | | | | |

Figure 6: Plate layout for the HTS of artificial sweeteners with the orphan receptors being placed in wells labeled R1-R8 and the controls of green fluorescent protein (GFP), pBluescript II SK+ (pBSK, NT) and Lysophosphatidic Acid Receptor 1 (LPA1) being placed on the sides.

Luciferase Assay

A plate containing cells from a previous experiment was thawed at room temperature and miliQ water was added to each well for a final dilution of 1:5. Working solution for the luciferase assay was prepared using 10 $\mu\text{g}/\mu\text{L}$ D-Luciferin stock and luciferase assay buffer. The lysate was added to a 384-well fluorescence white plate; miliQ water and working solution was also added to each well. Solution was incubated for five minutes with oscillation. Luminescence was then read on a Biotek Synergy HT Multimode Microplate reader.

β -Galactosidase Assay

The lysate from above was added to a clear 96-well plate with 2X β -Gal assay buffer (*o*-nitrophenyl- β -d-galactopyranoside). The plate was incubated at room temperature for 5-15 minutes depending on the quickness of the luminescence and then read at 420 nm in a SpectraMax spectrophotometer.

MTT Assay

0.1 µg of MTT was added to each well and incubated for 2-3.5 hours at 37°C. The media was then removed and DMSO was added to each well. It was placed on an orbital shaker for 15 minutes and protected from the light. Absorbance was then read at 570 nm in a SpectraMax spectrophotometer.

Green Fluorescent Protein Microscopy

GFP was used to determine how well transfection happened. GFP efficiency was calculated by hand, using pictures collected on the EVOS microscope under GFP conditions and transient conditions to determine the percentage of GFP transfection

$$(\text{Percentage GFP Transfection} = \frac{\text{GFP Cells}}{\text{Total Cells}}).$$

Data Analysis

All statistics and plotting were carried out in Prism 8 software (GraphPad Software; San Diego, CA, USA), or R Studio (Boston, MA, USA). For the transfected Tango assays, the procedure was carried out in triplicate and presented as fold change over non-transfected control. Data is presented as mean ± SEM. Relative light units (RLU) was determined from taking the luciferase data and normalizing the data with the β-Gal data for each receptor. Shapiro test, Bartlett's test, T-test, and Mann-Whitney U test were used to determine normal distribution, equal variance and statistical significance of comparisons between vehicle and treatment groups.

Results

Optimization of High Throughput Screen

To properly run an HTS of the artificial sweeteners, a series of optimization tests needed to be completed to make sure there would be no faulty reading because of controls, cell

concentration, reagents or even the plate layouts. To determine the optimal volumes of lysate sample and luciferin to use in the 384-well plate format, optimization of the luciferase assay was preformed with LPAR1 and LPAR2 using six different treatments with varying amounts of sample, water and working solution for the luciferase assay. Each receptor had three different conditions of FBS: vehicle, 10% FBS and then 20% FBS. Luminescence was quantified using a BioTek Synergy Multimode Microplate Reader and a SpectraMax spectrophotometer to compare reader performance. It was determined that the optimum ratio of sample to water to working solution was 10 μ L to 10 μ L to 10 μ L as it had the highest output (Figure 7). The fold change for this ratio was determined to be 2.80 and 3.90 for 10% FBS and 20% FBS on LPAR1 and 3.39 and 7.33 for 10% FBS and 20% FBS on LPAR2 using the Biotek reader; while it was 3.59 and 4.61 for 10% FBS and 20% FBS on LPAR1 and 2.64 and 6.49 for 10% FBS and 20% FBS on LPAR2 using the SpectraMax. Based from the RLU values and not the fold change, it was determined that the BioTek microplate reader gave stronger results as the highest RLU value was 7544.67 ± 205.90 while the SpectaMax only went as high as 218.43 ± 7.59 .

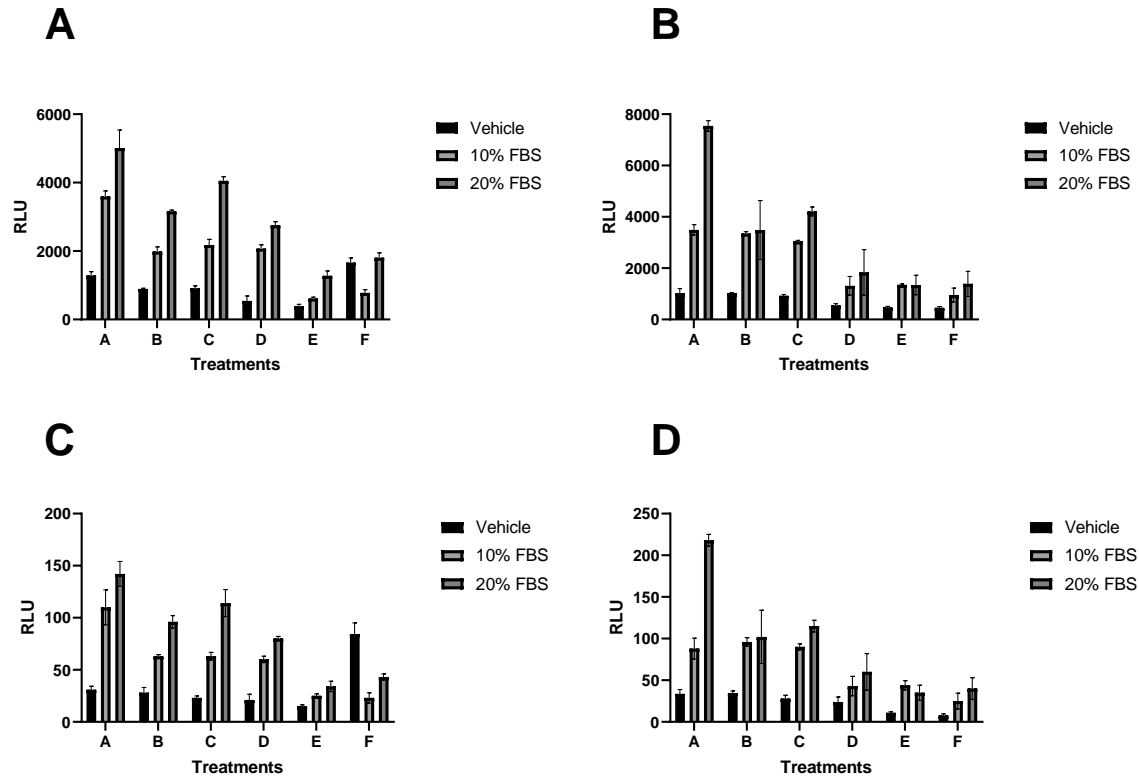


Figure 7: The optimization of lysate sample and luciferin working solution using a BioTek plate reader to measure LPAR1 (A) and LPAR2 (B) luminescence and a SpectraMax reader to measure LPAR1 (C) and LPAR2 (D) luminescence via a vehicle, 10% FBS and 20% FBS samples. Treatment ratios of lysate sample, water and working solution in μL are as follows: A – 10:10:10, B – 10:5:15, C – 10:0:20, D – 5:15:10, E – 5:10:15, F – 5:5:20. Data are shown as mean \pm SEM, where N=3.

LPAR1 and LPAR2 receptors were used as controls to optimize the performance of the PRESTO-Tango screen protocol (Figure 8). Cells transfected with LPAR1 had a RLU ($\frac{\text{luminescence}}{A420}$) of 1125.6 ± 147.6 for vehicle, 10% FBS of $24\,963.5 \pm 1847.9$ and 20% FBS of $24\,021.9 \pm 6337.6$ (Figure 8 A, B). This represents a fold change of 22.2 ± 4.0 for 10% FBS and 21.4 ± 2.6 for 20% FBS. The magnitude of the LPAR2 was less than that of LPAR1 with the vehicle having 308.8 ± 24.7 RLU, 10% FBS having 1431.2 ± 344.7 and 20% FBS having 1647.5 ± 199.5 . Showing a fold change of 4.6 ± 1.2 for 10% FBS and 5.3 ± 0.8 for 20% FBS (Figure 8

C, D); thus the vehicle of LPAR1 will be used with a BioTek plate reader as it has the RLU value and the lowest standard error.

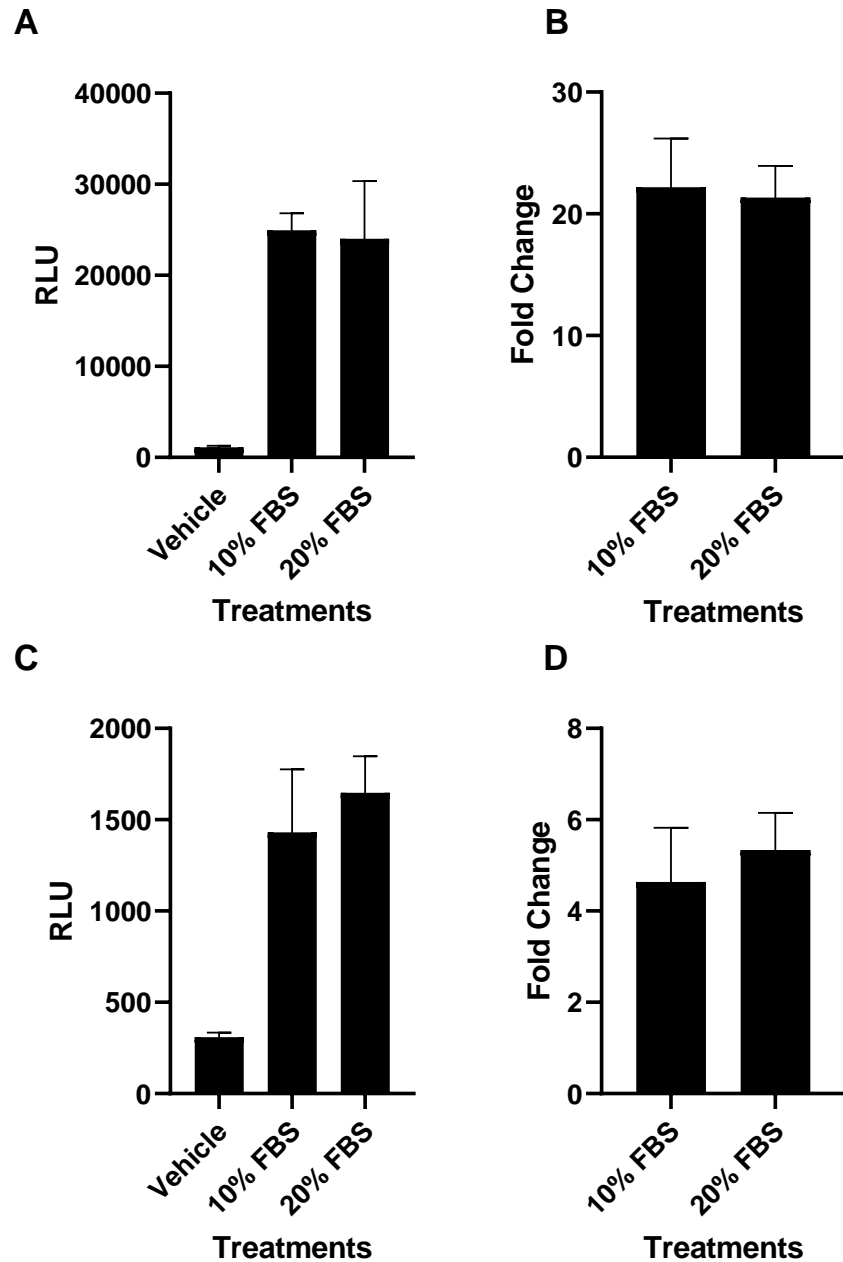


Figure 8: Determination of optimal positive control receptor and treatment conditions for PRESTO-Tango screen protocol (A) and fold change (B), and LPAR2 RLU values (C) and fold change (D). The graph is plotted with the treatments of the receptor against the RLU of each receptor found by a Luciferase assay and β -Gal assay. Data are shown as mean \pm SEM, where N=3.

To optimize DNA transfection conditions for HTS, the PEI reagent was added at varying amounts of 0.00, 0.05, 0.1, 0.2, 0.3 and 0.4 μL per well in combination with a beta-galactosidase expression vector. β -Galactosidase activity was quantified using our β -Gal assay to determine at what PEI concentration the best transfection efficiency took place. Absorbance at 420 nm was measured following 5, 10, 20 and 30 minute incubation of lysate with β -galactosidase substrate (Figure 9). The greatest change in absorbance at 420 nm at all four-time intervals was observed with 0.3 μL of PEI per well of HTLA cells. The transfection efficiency was assessed by microscopy in HTLA cells transfected with a GFP expression vector (Figure 10). It was determined that the GFP transfection efficiency was highest at 0.3 μL of PEI per well giving a transfection efficiency of $24.6 \pm 2.1\%$.

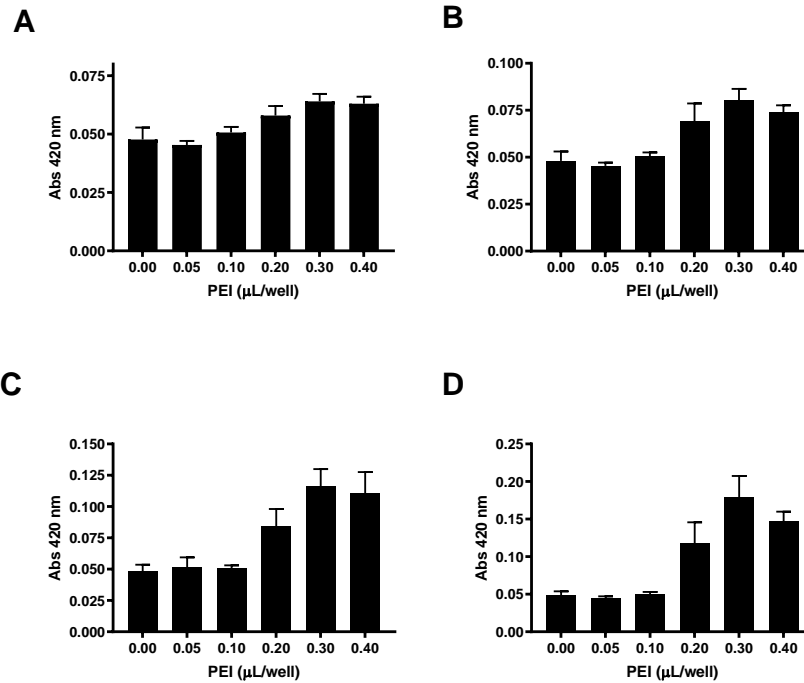


Figure 9: The optimization of PEI reagent using a β -Gal Assay (Absorbance at 420 nm) at four-time intervals; 5 minutes (A), 10 minutes (B), 20 minutes (C) and 30 minutes (D) against six different amounts of PEI that were added to each well. 0.3 μL was determined to have the largest absorbance in all four-time intervals. Data are shown as mean \pm SEM, where N=3.

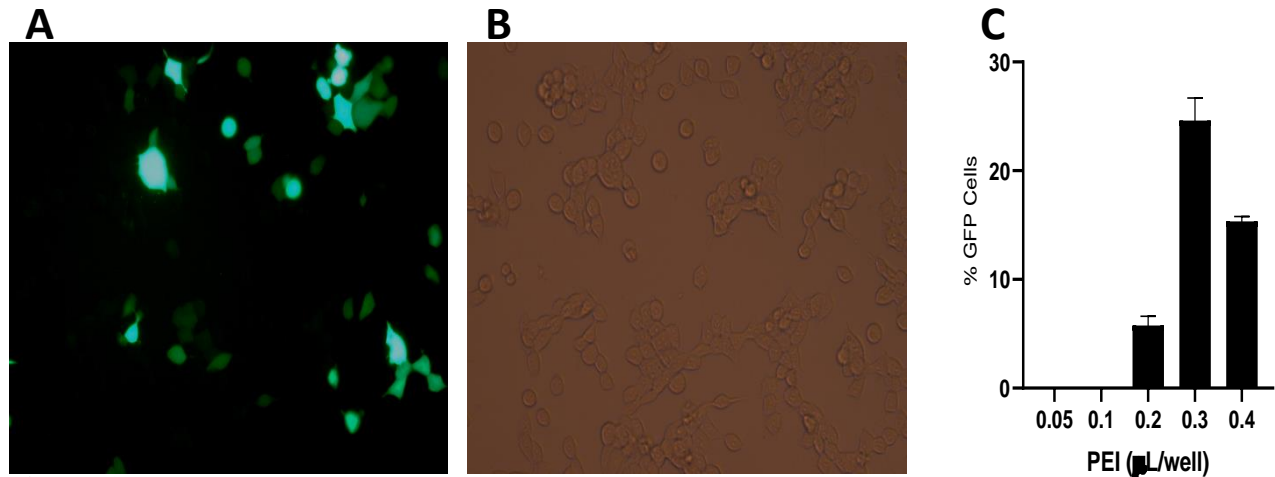


Figure 10: The GFP transfection efficiency percentage is based on the amount of PEI and how well it transfected the GFP plasmid (A) into the HTLA Cells (B). It was determined that 0.3 µL of PEI had the best GFP transfection percentage in comparison to the other amounts (C). Data are shown as mean ± SEM, where N=3.

Another PEI optimization was done as it was found that as the amount of cells plated per well increases, the reagents act differently, so an experiment with varying amounts of PEI and varying plated cell numbers was performed to determine the optimal concentration for both. Cells plated at or below 20 000 cells per well had shown the best transfection efficiency and PEI of 0.2 or 0.3 µL per well had the lowest standard error of the mean when calculating the percentage of GFP transfected (Figure 11).

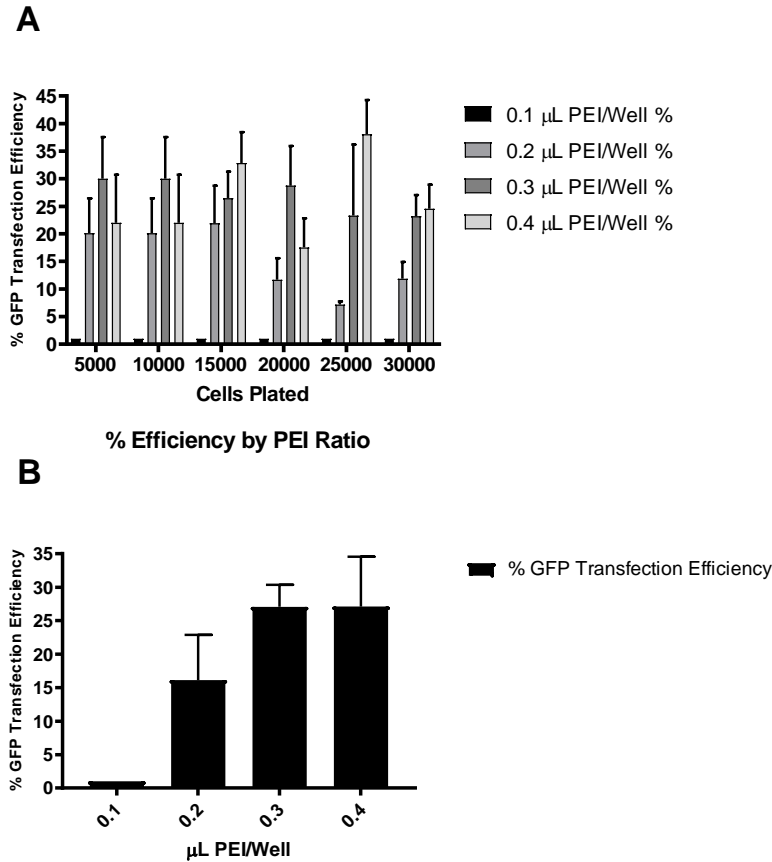


Figure 11: PEI optimization with varying amounts of HTLA cells plated per well. It was concluded that keeping the cells plated at or below 20 000 cells per well leads to the least amount of variability between sets (A). Wells with 0.3 μL PEI leads to the greatest percentage of GFP transfection with $27.1 \pm 1.3\%$ (B). Data are shown as mean \pm SEM, where N=3.

Contamination Testing

During the duration of this study, there had been multiple outbreaks of contamination with the HTLA cells. It was therefore necessary to ensure the HTLA cells were contamination-free prior to use in screening. Mycoplasma infection is a common source of cell culture contamination that interferes with many cellular measurements. Mycoplasma contamination can be easily spotted using a DAPI nuclear DNA stain, where mycoplasma appear as small extranuclear puncta. There was no evidence of mycoplasma in the HTLA cells. Another outbreak of small circular bodies was also routinely observed in the cells after transfection and an

experiment that used an old and new solution of PEI, Opti-MEM and Complete DMEM was created to find if any of these were a source of microbial contamination. It was determined that the PEI that we received from a new supplier was causing the small apoptotic bodies to break off from the cells after 24 hours post transfection and that these were eliminated using a shorter transfection time of 12-18 hours. This was done by looking at the cells under the EVOS microscope to determine if the bodies were there at the given time (Figure 12).

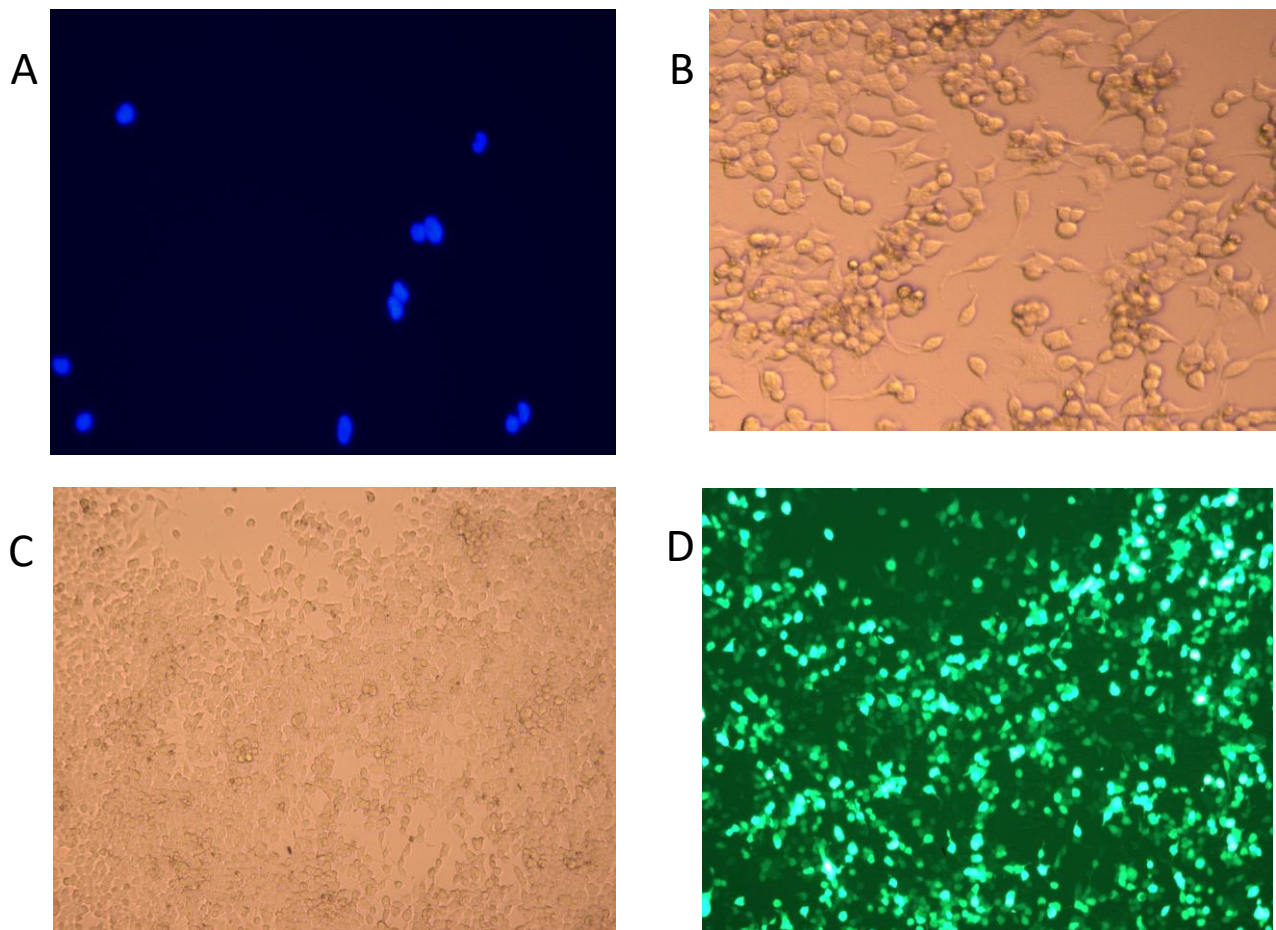


Figure 12: Contamination testing revealed that there was no mycoplasma within the HTLA cell line (A). Running the PEI contamination test found that apoptotic bodies formed from the PEI after 24 hours of transfection (B). When completely optimized the normal HTLA cells (C) should yield high transfection efficiency shown by GFP (D).

High Throughput Sweetener Screen

Once the optimization for the screen was completed, a high throughput PRESTO-TANGO screen was performed with 72 orphan receptors (Table 1) treated with vehicle or a combination of the artificial sweeteners aspartame and acesulfame potassium at a concentration of 6 mM and 3 mM, respectively; as determined from the study done by van Eyk *et al.* 2015 Five replicates (sets) of orphan receptor screens were completed. On every receptor plate, there was an LPAR1 control positive and negative group that were used to determine if the transfection worked properly and to verify any receptor hits that the screen could get. The RLU and fold change of each LPAR1 control across the four sets show how well the screen performed (Figure 13). One replicate (Set B) that did not respond to positive control treatments was excluded from future analysis. Set A had a fold change average of 1.74 ± 0.39 with the highest being 2.36 ± 0.13 on plate 2 and the lowest being 1.28 ± 0.13 on plate 7. Set C had a fold change average of 2.33 ± 0.83 with the highest being 3.79 ± 0.27 on plate 7 and the lowest being 0.96 ± 0.28 on plate 3. Set D had a fold change average of 7.63 ± 2.04 with the highest being 11.96 ± 0.86 on plate 7 and the lowest being 5.20 ± 0.68 on plate 2. Set E had a fold change average of 5.05 ± 1.84 with the highest being 7.57 ± 0.61 on plate 6 and the lowest being 2.59 ± 0.63 on plate 4. This shows that the control group of LPAR1 had similar values across the replicates of the sets completed.

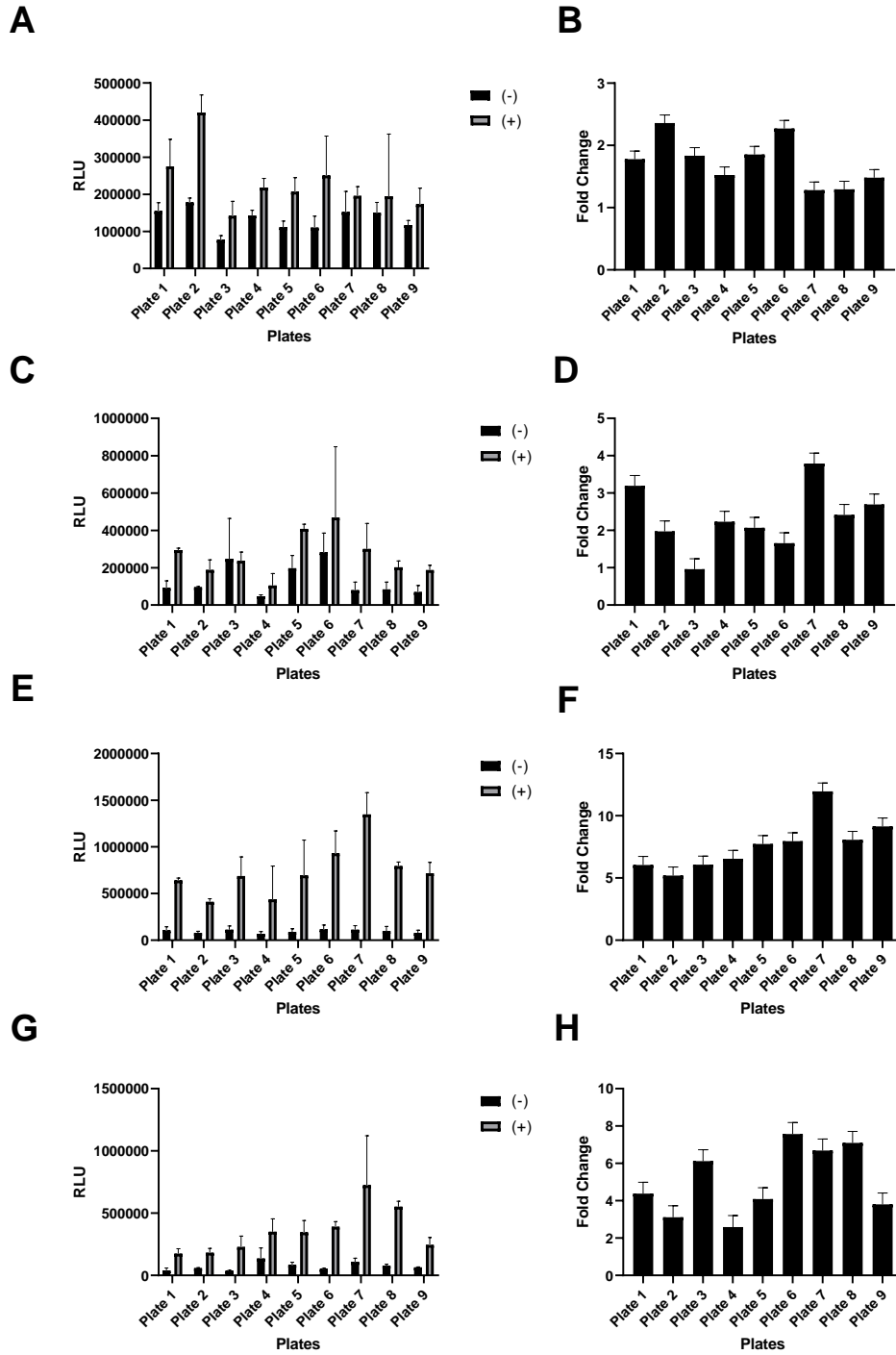


Figure 13: The LPAR1 controls of the HTS that show the RLU and fold changes per plate that are used to compare to potential orphan receptor hits. Orphan screen Set A RLU (A) and fold change (B), orphan screen Set C RLU (C) and fold change (D), orphan screen Set D RLU (E) and fold change (F), and orphan screen Set E RLU (G) and fold change (H). Data are shown as mean \pm SEM, where N=3.

The data from the screen was entered in an excel file that was reformed and corrected the luminescence value with the β -Gal assay values to create the RLU which could then be put into R Studio to find the values for the Shapiro test, Bartlett's test, T-test, and Mann-Whitney U test for each orphan receptor. From these values it was determined if the receptor values were normally distributed, of equal variance and lastly if there was a significant response or not. The inverse significance value was then plotted on a heatmap to see how the receptors acted across the four screens (Figure 14). From the analysis performed, it was determined that only one receptor had significance across the four screens and that was R37, which correlates to GPR32. Across the four sets A, C, D and E, GPR32 had a fold change of 1.37 ± 0.18 , 0.51 ± 0.18 , 0.47 ± 0.11 , and 0.37 ± 0.09 , respectively (Figure 15). The sweetener mix was found to decrease activation in GPR32 in Sets C, D and E while increasing it in Set A.

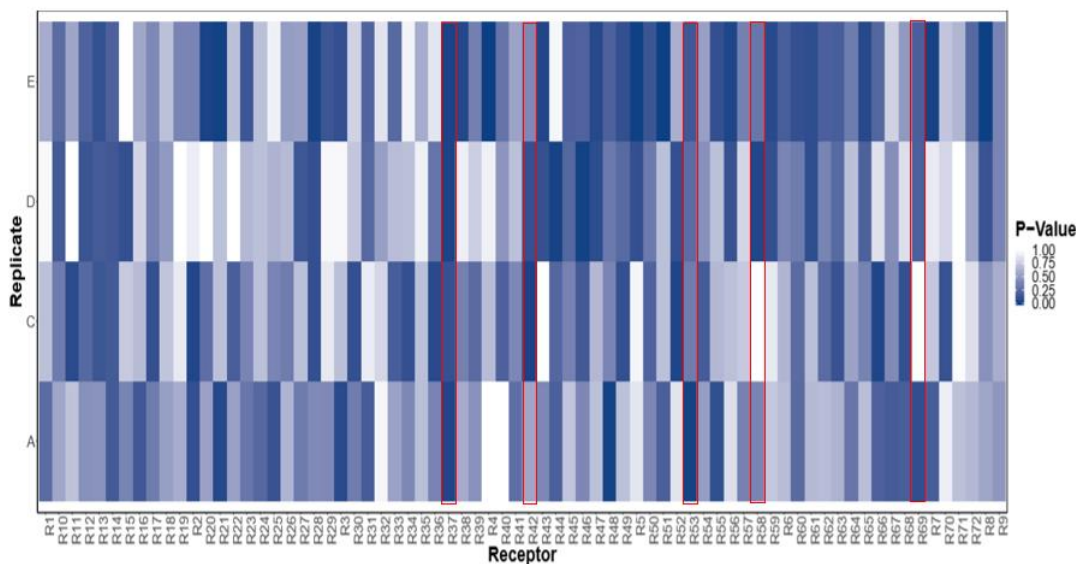


Figure 14: A heatmap diagram of orphan receptors treated with an aspartame and acesulfame potassium mixture. The significance level (p-value) is of the change in luminescent signaling between the NNS treatments and Opti-MEM control for the 72 orphan receptors. The four biological replicates are signified as A, C, D and E. R7 (GPR12), R37 (GPR32), R42 (GPR4), R53 (GPR84) and R58 (MAS1) are highlighted in red, as they were deemed to have a significant change in luminescence.

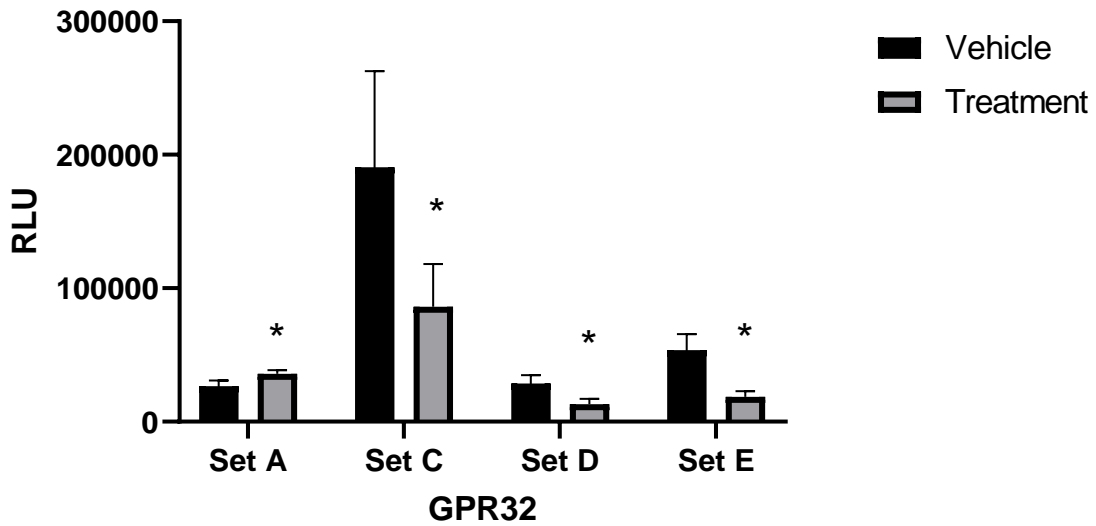
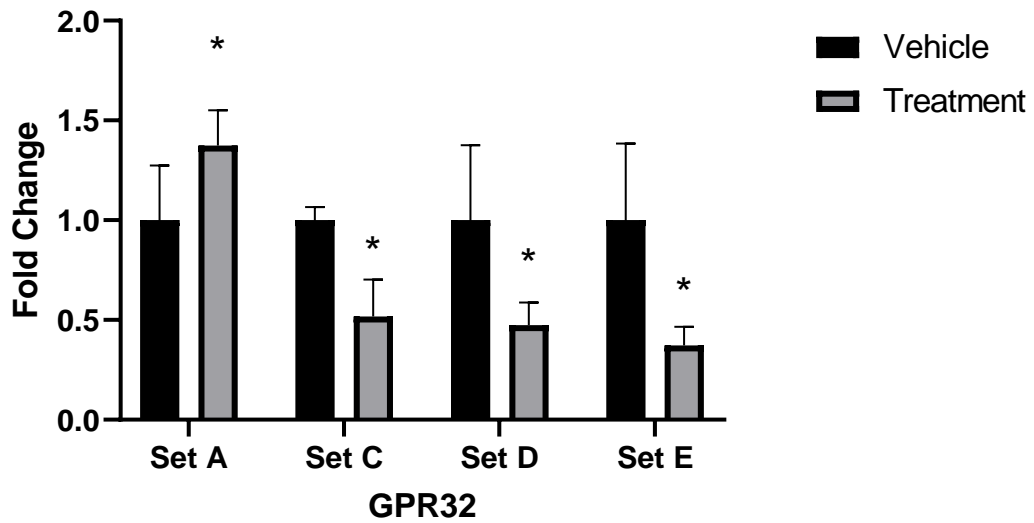
A**B**

Figure 15: RLU (A) and fold change (B) for GPR32 when treated with 3X artificial sweetener mixture containing aspartame and acesulfame potassium relative to the vehicle treatment. Shapiro test, Bartlett's test, T-test, and Mann-Whitney U test showed that there was significance ($p < 0.05$) between sweetener and control treatments as shown with an asterisk (*). Data are shown as mean \pm SEM, where $N=3$.

There were however, 18 other orphan receptors that had a significant difference in at least one set between vehicle and sweetener mix, based on if there was significance in more than one set or if there was an increase or decrease in activation in multiple sets; four additional receptors that warrant further investigation are shown in greater detail. These receptors are GPR12 (R7), GPR4 (R42), GPR84 (R53) and MAS1 (R58). GPR12 had a fold change that was significantly different in 2 of the 4 sets (2.17 ± 0.82 , 0.227 ± 0.002) with one showing an increase and the other a decrease (Figure 16). The sweetener mix was found to decrease activation in GPR12 in Sets E while increasing it set A, with it being found significant in Set D and A.

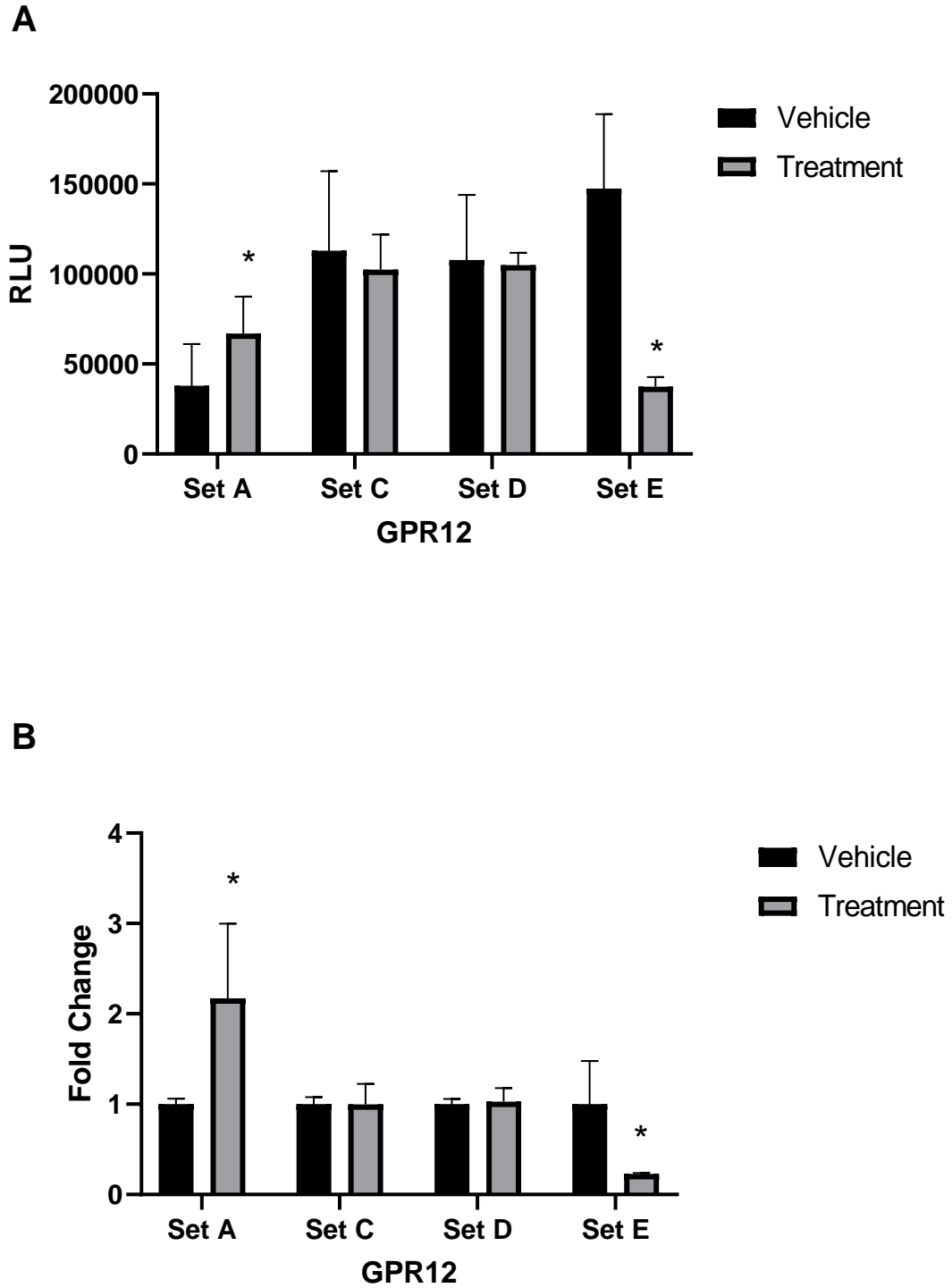


Figure 16: RLU (A) and fold change (B) for GPR12 when treated with 3X artificial sweetener mixture containing aspartame and acesulfame potassium relative to the vehicle treatment. Shapiro test, Bartlett's test, T-test, and Mann-Whitney U test showed that there was significance

GPR4 had a fold change of 1.90 ± 1.15 , 2.06 ± 0.38 , 1.67 ± 0.21 , and 0.59 ± 0.25 , respectively (Figure 17). The sweetener mix was found to increase activation in GPR4 in Sets A, C, and D, with it being found significant in Set C. GPR84 had a fold change of 2.11 ± 0.34 , 0.90 ± 0.39 , 1.55 ± 0.44 , and 2.97 ± 1.60 , respectively (Figure 18). The sweetener mix was found to increase activation in GPR84 in Sets A, D, and E while decreasing it in set C, with it being found significant in Set A. The last orphan GPCR is MAS1 which had a fold change of 3.41 ± 1.80 , 1.08 ± 0.14 , 2.13 ± 0.38 , and 1.36 ± 0.23 , respectively (Figure 19). The sweetener mix was found to increase activation in MAS1 in sets A and D, with it being found significant in Set A and D. Collectively, this preliminary data shows that through the PRESTO-Tango method, artificial sweeteners can be used as a possible ligand for some orphan GPCRs.

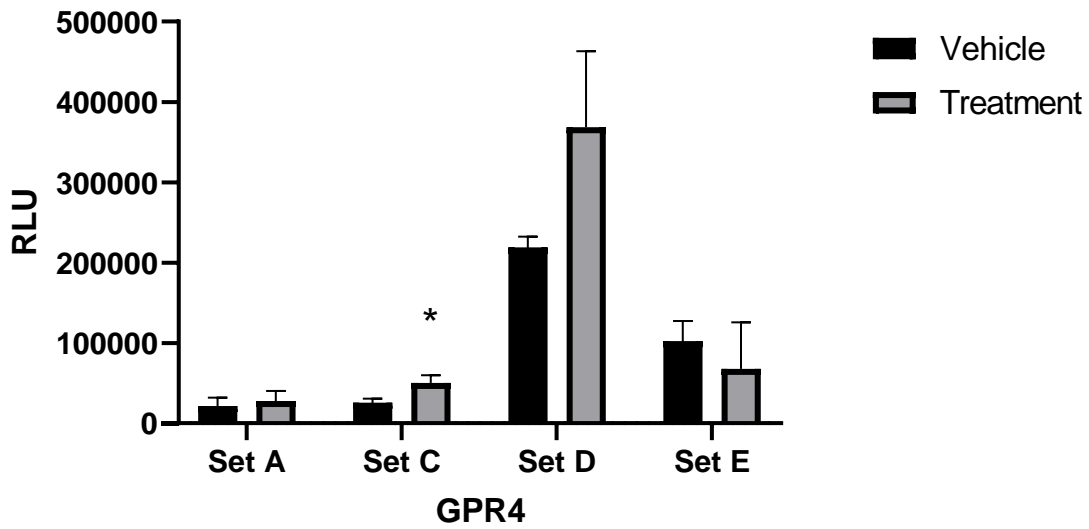
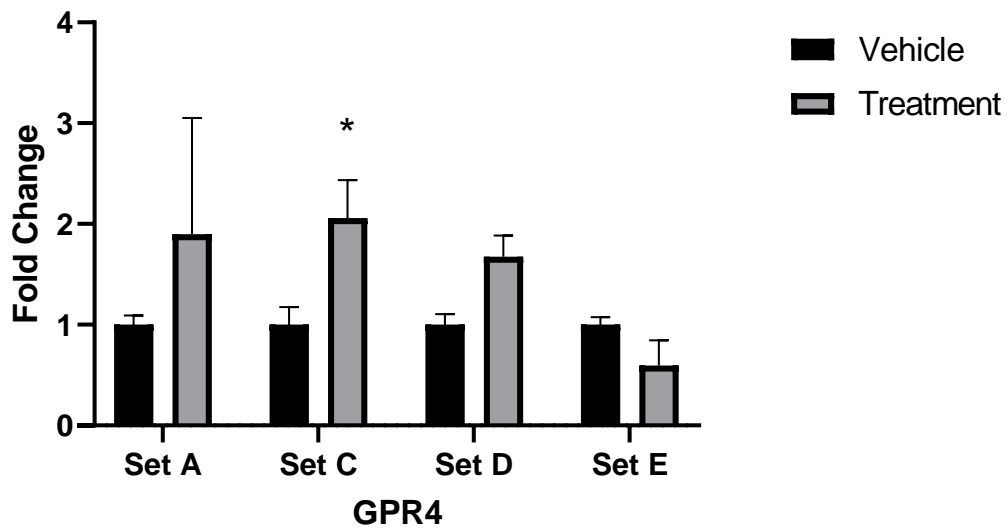
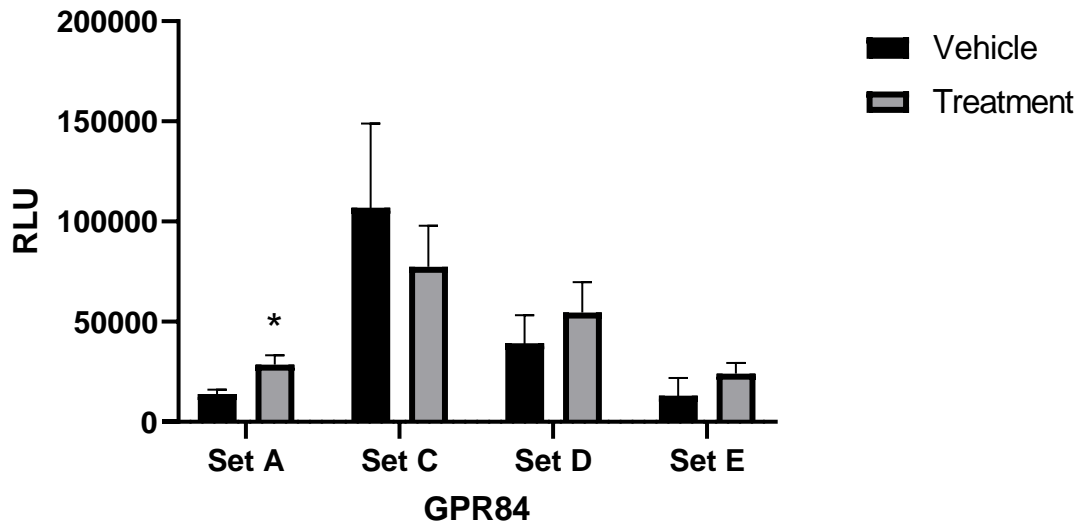
A**B**

Figure 17: RLU (A) and fold change (B) for GPR4 when treated with 3X artificial sweetener mixture containing aspartame and acesulfame potassium relative to the vehicle treatment. Shapiro test, Bartlett's test, T-test, and Mann-Whitney U test showed that there was significance ($p < 0.05$) between sweetener and control treatments as shown with an asterisk (*). Data are shown as mean \pm SEM, where $N=3$.

A



B

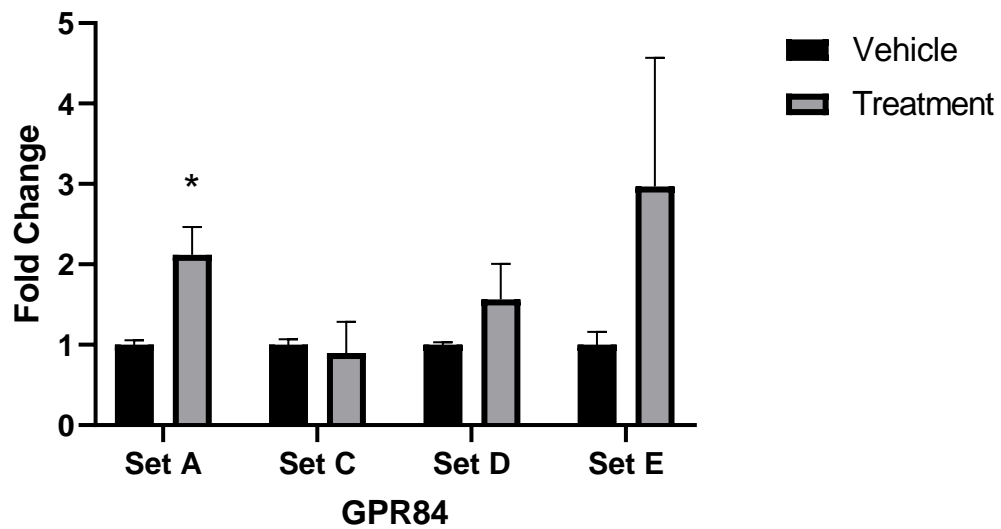


Figure 18: RLU (A) and fold change (B) for GPR84 when treated with 3X artificial sweetener mixture containing aspartame and acesulfame potassium relative to the vehicle treatment. Shapiro test, Bartlett's test, T-test, and Mann-Whitney U test showed that there was significance ($p < 0.05$) between sweetener and control treatments as shown with an asterisk (*). Data are shown as mean \pm SEM, where N=3.

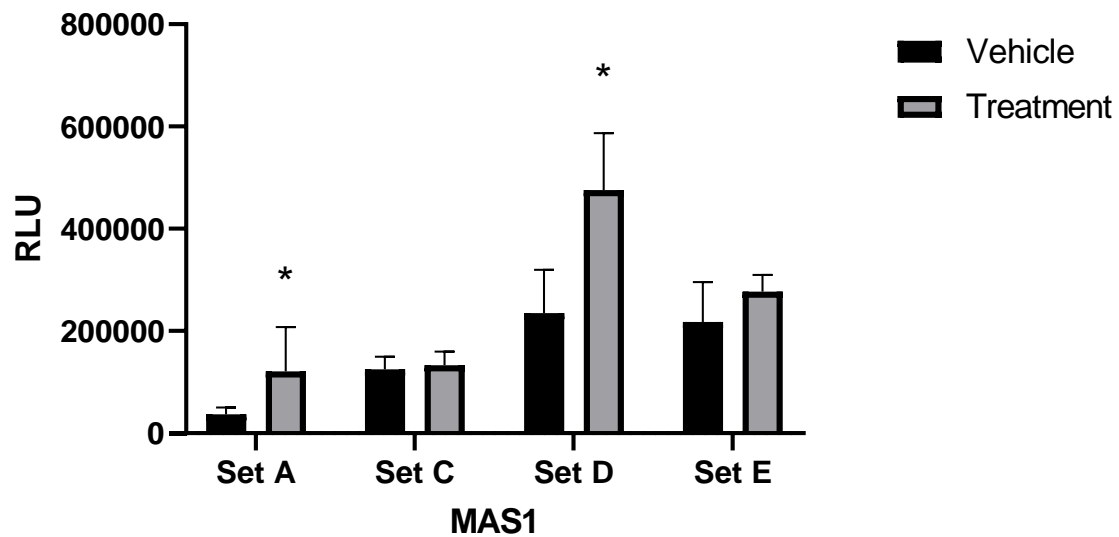
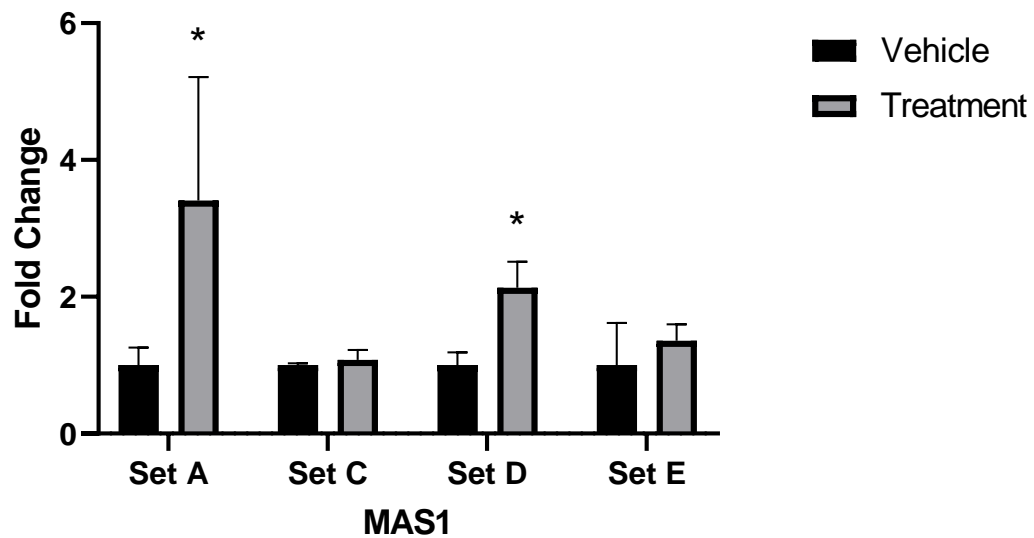
A**B**

Figure 19: RLU (A) and fold change (B) for MAS1 when treated with 3X artificial sweetener mixture containing aspartame and acesulfame potassium relative to the vehicle treatment. Shapiro test, Bartlett's test, T-test, and Mann-Whitney U test showed that there was significance ($p < 0.05$) between sweetener and control treatments as shown with an asterisk (*). Data are shown as mean \pm SEM, where $N=3$.

Discussion

The goal of this study was to determine if the artificial sweeteners aspartame or acesulfame potassium would activate or inactivate any of the 72 orphan class A receptors that were chosen to be a part of this experiment (full list in supplementary section). This was done by running a PRESTO-Tango high throughput screen that measures the β -arrestin recruitment by the receptor once the ligand binds. To get the screen optimized there were a series of experiments that were first performed.

Optimization of High Throughput Screen

The optimization of the high throughput screen showed that it is possible to get up to a 20-fold activation through LPAR1 using 10% FBS media and the correct concentrations of reagents. It was also found that the 384-well plate needed the optimum ratio of lysate, buffer, and water of 10:10:10 μ L to yield the highest RLU values possible. The PEI was also optimized to be 0.3 μ L per well of cells. Having the optimum amount of PEI allows for micelles to form allowing the transfection efficiency to be at its best (Smale, 2010). It was also determined that cells needed to be plated at/or under 20 000 cells per well at a low confluency (around 60%) because the more confluent the cells are, the harder it is to get strong transfection efficiency (Rybakovsky *et al.* 2019).

Contamination Testing

A DAPI luminescence test was performed to determine if the cells were contaminated with mycoplasma. Mycoplasma is one of the most prevalent lab contaminations and can render data unusable, induce cellular change, and allow cells to gain resistance to chemotherapeutic drugs (Yin *et al.* 2019). It was determined that there was no mycoplasma, that it was a high number of passages for the cell line which caused the effects on transfection efficiency, cell

growth, and plating efficiency (Chang-Liu and Woloschak, 1997). A second contamination occurred where it was determined via EVOS microscope, that small apoptotic bodies from the cells would break off due to the PEI after 24 hours of transfection. PEI is a polymer that can condense plasmid DNA into nano-sized polyplexes; however, it has a high cytotoxicity (Kara *et al.* 2018). A lower concentration of PEI was used, and transfection was completed after 12-18 hours of incubation, stopping the formation of apoptotic bodies.

High Throughput Sweetener Screen

Originally there were five sets of screen data, where the first three sets (A, B and C) were done completed but more test needed to be completed as set B did not work properly so, sets D and E were then completed. The reasoning for this is that Set B did not have useable LPAR1 control data and the transfection did not work properly. This is believed to have happened because the cells were getting higher in passage number and did not plate overly well for Set B and C, with Set C having 48 hours of incubation after plating to help grow the cells. Since there was no LPAR1 control data, the plate could not be used and was excluded from the study. Poor condition of cells in Set A and C is also why the fold change is for those two sets combined is 68% lower than the fold change for Set D and E combined. The cells for Sets D and E were passaged three times before plating and allowed the cells to transfect extremely well and had the largest fold change of the screen data that was studied. Together these findings suggested that to run a high throughput screen a new cell line must be brought up, passaging can only take place twice or three times, then the screen must be completed to maintain high quality screens and reliable data.

The screen data showed that there are 5 possible receptors whose activity is altered in response to artificial sweeteners: GPR32, GPR4, GPR12, GPR84 and MAS1. Given the

variability observed between screen replicates, validation experiments are ongoing to determine if the artificial sweetener aspartame or acesulfame potassium is the ligand. The screen data provided valuable preliminary data on each of the five receptors as potential receptors for artificial sweeteners.

In this study, GPR32 was the only receptor to show a p value < 0.05 in all sets and had down regulation in Sets C, D, and E, respectively; with the first set A showing an up regulation in activity. GPR32 is an orphan receptor that has been linked to a few functions using Resolvin D1 (RvD1), an enzymatic derivative of docosahexaenoic acid (Sun *et al.* 2007). GPR32 is expressed in human leukocytes and adipose tissue and has been linked to inducing pro-resolution macrophage phenotype with reduction to proinflammatory cytokines (Schmid *et al.* 2016). GPR32 has also been linked to inflammatory signalling in airway epithelial cells by trying to inhibit RvD1 (Hsiao *et al.* 2014). It has also been linked to lung cancer by using RvD1 as an inhibitor. With the preliminary findings showing that GPR32 is down regulated in three sets, NNS could potentially be used to inhibit the receptor which has been linked to in the epithelial cells of the inflammatory signalling pathway. A549 lung cancer cells also are linked to the inhibitory nature of GPR32 and with the sweeteners down regulating it there could also be an interaction there as well. This means that the artificial sweeteners potentially inhibit the GPR32 in lung cancer as well as act as an inflammatory signal with the receptor.

In this study, GPR4 was significant in Set C with it having an increase in activation. GPR4 has been characterized as a novel pH sensor that is proposed to be activated by acidic extracellular pH, is overexpressed in various malignancies, may be involved in cancer-related angiogenesis (Jing *et al.* 2016), and plays a role in promoting colorectal cancer progression by activating the hippo pathway (Yu *et al.* 2019). GPR4 is also found in endothelial cells for ER

stress pathways and tube formation of blood vessels (Ren *et al.* 2016 and Dong *et al.* 2017). GPR4 has also been suggested to play a critical role in the inflammatory responses activated by lysophosphatidylcholine (LPC) where it has been found in epithelial cells and associated with diseases like asthma (Qiao *et al.* 2006 and Lum *et al.* 2003). With the knowledge that GPR4 has been activated in these pathways, it is possible based on the preliminary findings that artificial sweeteners could be linked to cancer-related angiogenesis, colorectal cancer in the activation of the hippo pathway and playing a role in the inflammatory responses in diseases like asthma due to their activation of GPR4 shown in this study.

GPR12 was activated in Set A and decreased activation in Set E, respectively. GPR12 is believed to be a peptide and lipid receptor (Ignatov *et al.* 2003) that is a constitutively active GPCR. It has been linked to brain development, metastatic cancer (Brown *et al.* 2017), cell proliferation, and signal transduction to activate the ERK $\frac{1}{2}$ pathway, a key pathway in the promotion of cell proliferation (Lu *et al.* 2012) and is expressed in umbilical endothelial cells (Uhlenbrock *et al.* 2003). GPR12 is also believed to be coupled to an inhibitory G-protein. It is very possible that this receptor is activated by aspartame as it is believed to be a peptide receptor (Ignatov *et al.* 2003). Given that aspartame breaks down into phenylalanine (50%), aspartic acid (40%) and methanol (10%), each of the two amino acids can potentially bind to GPR12. Aspartame is metabolized in the stomach; however, the metabolites travel through the bloodstream and could potentially find a GPR12 receptor in the epithelial cells along the brain. This receptor, however, needs more verification due to one of the screens showing an increase, one showing a significant decrease and then two sets not showing any activation at all.

GPR84 is a putative receptor for medium fatty acid chains and has been suggested as a novel target to treat chronic low-grade inflammatory diseases (Suzuki *et al.* 2013). It has also

been shown to trigger bacterial adhesion in macrophages and enhance the inflammation signal once it is established (Recio *et al.* 2018). In this study, GPR84 had an increase in activity in three sets: A, D, and E. This data shows that it is possible that the agonist for GPR84 could be an artificial sweetener as the receptor has been found in epithelial cells and artificial sweeteners have to travel through the bloodstream and could bind with them. Also, the activation of GPR84 in this study could potentially lead to linking artificial sweeteners to enhancing an inflammation signal once its been activated.

High expression of MAS1 in the inner lining of the uterus has been suggested to promote endometriosis (Nakajima *et al.* 2018). Mas1 is known to be a receptor for angiotensin 1 through 7 and induces vessel dilation and depression of blood pressure, as well as being negatively associated with breast cancer by inhibiting cell growth and anti-apoptotic survival signals and therefore could make MAS1 an inhibitory regulator of breast cancer (Luo *et al.* 2015). MAS1 is also believed to be a receptor for peptide ligands similarly to that of GPR12 (Tirupula *et al.* 2014). Since this could be a peptide receptor, its possible that aspartame could be the ligand since the metabolites break down into two amino acids. Also, MAS1 was activated in all four sets of this study suggesting that there is a strong chance that aspartame could be the ligand for this receptor.

Its worth noting that all five of the receptors have the ability to come into contact with an artificial sweetener in the body because they all are found within epithelial cells that gives them access to the bloodstream where the artificial sweeteners go to travel through the body. It is also very intriguing that GPR4, GPR32, and GPR84 all in some way are connected to inflammatory responses. Artificial sweeteners, especially aspartame and acesulfame potassium, cause

inflammation in the body (Hall *et al.* 2017 and Bian *et al.* 2017) which leads me to believe that these are actual hits and not false positives.

Artificial sweeteners have been linked to inflammation in a few studies that state that the sweeteners have been found to cause glucose intolerance and induce metabolic syndrome which leads to a higher risk in obesity. In these cases, it's been found that artificial sweeteners can disrupt the gut microbiome which can produce pro-inflammatory mediators (Bian *et al.* 2017 and Ruiz-Ojeda *et al.* 2019). In the Bian *et al.* study they looked at the disruption that led to the eliciting of inflammation; with the three receptors being linked to inflammation in this study, it is possible that the artificial sweeteners themselves bind to the receptor that cause the inflammatory responses seen in previous studies, instead of a disruption that leads to the inflammation.

The other two receptors, GPR12 and MAS1, also share a similar trait and that's both receptors are believed to be peptide receptors meaning aspartame could also bind to them as well due to the metabolites that it breaks up into in the digestive tract. The break down of these metabolites generally are toxic in high dosages but the amount consumed is usually never high enough to find an effect (Pradhan *et al.* 2010). If the prolonged use of artificial sweeteners caused a build up of effect of formaldehyde, the metabolite, which was seen in a small-scale experiment done by Tandel, 2011 then this study could be the building block to prove this correct. With both GPR12 and MAS1 being linked to cancer, it is possible that the metabolite formaldehyde of aspartame plays a role in its development because it is a known carcinogen for humans (Kwon *et al.* 2018). More research is needed in this field to truly understand the long term affects of artificial sweeteners, but this becomes a step in the right direction.

Conclusion and Future Directions

The aim of this study was to determine if the artificial sweeteners, aspartame and acesulfame potassium, would bind to any of the 72 class A orphan receptors using the PRESTO-TANGO high throughput screening method. After optimizing the screen and dealing with contamination on multiple occasions, it was determined through preliminary trials that five receptors: GPR4, GPR12, GPR32, GPR84 and MAS1 have a significant change in sweetener treatment and vehicle control. Validation is required to ensure these findings represent true hits and not artifacts or false positives.

Validation of the five receptors will require treating each with individual sweeteners and not a mix. This will allow us to fully determine if there was an actual hit and by which artificial sweetener. If a true positive hit does emerge from this validation, then a dose response curve will need to be done with that receptor and artificial sweetener. This will then be followed up by verifying that the ligand does activate or inactivate the receptor by using another signalling pathway that isn't the β -arrestin pathway. One pathway to use could be the Ca^{2+} pathway; once that is completed and the receptor is validated then a more human nature body environment model will need to be designed due to the PRESTO-Tango method actively recruiting arrestin which could give off a false signal, which the body doesn't do, so a more natural human body model is needed. An experiment would then be needed to determine how and where the ligand binds on the receptor. This study will further advance our knowledge that Class A GPCRs might be a target for artificial sweeteners. This is an important finding as it was believed that only the taste receptors in Class C were the receptors for sweeteners. It also allows for some GPCRs to be removed from the orphan list and individual research can be done on each receptor to determine their role with artificial sweeteners and the long-term metabolic effects that they might have.

Literature Cited

- Alexander, S.P.H., Christopoulos, A., Davenport, A.P., Kelly, E., Marrion, N.V., Peters, J.A., Faccenda, E., Harding, S.D., Pawson, A.J., Sharman, J.L., Southan, C., Davies, J.A.; CGTP Collaborators. The Concise Guide to PHARMACOLOGY 2017/18: G protein-coupled receptors. *Br J Pharmacol.* 2017; 174 Suppl 1: S17-S129.
- Allen, J.A., Halverson-Tamboli, R.A., Rasenick, M.M. Lipid raft microdomains and neurotransmitter signalling. *Nat Rev Neurosci.* 2007;8(2):128-140.
- Barnea, G., Strapps, W., Herrada, G., Berman, Y., Ong, J., Kloss, B., Axel, R., Lee, K.J. The genetic design of signaling cascades to record receptor activation. *Proc Natl Acad Sci U S A.* 2008; 105(1): 64-69.
- Bian, X., Chi, L., Gao, B., Tu, P., Ru, H., Lu, K. The artificial sweetener acesulfame potassium affects the gut microbiome and body weight gain in CD-1 mice. *PLoS One.* 2017; 12(6): e0178426.
- Brown, K.J., Laun, A.S., Song, Z.H. Cannabidiol, a novel inverse agonist for GPR12. *Biochem Biophys Res Commun.* 2017;493(1):451–454.
- Brown, R.J., de Banate, M.A., Rother, K.I. Artificial sweeteners: a systematic review of metabolic effects in youth. *Int J Pediatr Obes.* 2010; 5(4): 305–312.
- Chang-Liu, C.M., Woloschak, G.E. Effect of passage number on cellular response to DNA-damaging agents: cell survival and gene expression. *Cancer Lett.* 1997;113(1-2):77-86.
- Choudhary, A.K., Lee, Y.Y. Neurophysiological symptoms and aspartame: What is the connection?. *Nutr Neurosci.* 2018;21(5):306-316.

- Cong, X., Topin, J., Golebiowski, J. Class A GPCRs: Structure, Function, Modeling and Structure-based Ligand Design. *Curr Pharm Des.* 2017; 23(19): 4390-4409.
- Dong, L., Krewson, E.A., Yang, L.V. Acidosis Activates Endoplasmic Reticulum Stress Pathways through GPR4 in Human Vascular Endothelial Cells. *Int J Mol Sci.* 2017;18(2):278.
- Fredriksson, R., Lagerström, M.C., Lundin, L.G., Schiöth, H.B. The G-protein-coupled receptors in the human genome form five main families. Phylogenetic analysis, paralogon groups, and fingerprints. *Mol Pharmacol.* 2003; 63(6): 1256-1272.
- Gurevich, E.V., Gurevich, V.V. Arrestins: ubiquitous regulators of cellular signaling pathways. *Genome Biol.* 2006;7(9):236.
- Gurevich, V.V., Gurevich, E.V. Molecular Mechanisms of GPCR Signaling: A Structural Perspective. *Int J Mol Sci.* 2017;18(12):2519.
- Hall, L. N., Sanchez, L. R., Hubbard, J., Lee, H., Looby, S. E., Srinivasa, S., Zanni, M. V., Stanley, T. L., Lo, J., Grinspoon, S. K., Fitch, K. V. Aspartame Intake Relates to Coronary Plaque Burden and Inflammatory Indices in Human Immunodeficiency Virus. *Open forum infectious diseases.* 2017;4(2):ofx083.
- Hanlon, C.D, Andrew, D.J. Outside-in signaling--a brief review of GPCR signaling with a focus on the Drosophila GPCR family. *J Cell Sci.* 2015;128(19):3533–3542.
- Higgins J.B., Caseys P. J. In vitro processing of recombinant G protein γ subunits. *J. Biol. Chem.* 1994; 269:9067-9073.

- Hooper, N.M., Hesp, R.J., Tiekku, S. Metabolism of aspartame by human and pig intestinal microvillar peptidases. *Biochem J.* 1994;298:635–639.
- Hsiao, H.M., Thatcher, T.H., Levy, E.P., Fulton, R.A., Owens, K.M., Phipps, R.P., Sime, P.J. Resolvin D1 attenuates polyinosinic-polycytidylic acid-induced inflammatory signaling in human airway epithelial cells via TAK1. *J Immunol.* 2014;193(10):4980-7.
- Ibi, D., Suzuki, F., Hiramatsu, M. Effect of AceK (acesulfame potassium) on brain function under dietary restriction in mice. *Physiol Behav.* 2018; 188: 291-297.
- Ignatov, A., Lintzel, J., Hermans-Borgmeyer, I., Kreienkamp, H.J., Joost, P., Thomsen, S., Methner, A., Schaller, H.C. Role of the G-protein-coupled receptor GPR12 as high-affinity receptor for sphingosylphosphorylcholine and its expression and function in brain development. *J Neurosci.* 2003;23(3):907-14.
- Imada, T., Misaka, T., Fujiwara, S., Okada, S., Fukuda, Y., and Abe, K. Amiloride reduces the sweet taste intensity by inhibiting the human sweet taste receptor. *Biochemical and Biophysical Research Communications.* 2010;397:220–225.
- Jing, Z., Xu, H., Chen, X., Zhong, Q., Huang, J., Zhang, Y. The Proton-Sensing G-Protein Coupled Receptor GPR4 Promotes Angiogenesis in Head and Neck Cancer. *PLoS ONE.* 2016;11(4): e0152789.
- Kara, A., Ozturk, N., Esendagli, G., Ozkose, U.U., Gulyuz, S., Yilmaz, O., Telci, D., Bozkir, A., Vural, I. Development of novel self-assembled polymeric micelles from partially hydrolysed poly(2-ethyl-2-oxazoline)-co-PEI-b-PCL block copolymer as non-viral vectors for plasmid DNA in vitro transfection, *Artificial Cells, Nanomedicine, and Biotechnology.* 2018; 46:S264-S273.

- Kobilka, B.K. G protein coupled receptor structure and activation. *Biochim Biophys Acta*. 2006; 1768(4): 794–807.
- Kroeze, W.K., Sassano, M.F., Huang, X.P., Lansu, K., McCorvy, J.D., Giguère, P.M., Sciaky, N., Roth, B.L. PRESTO-Tango as an open-source resource for interrogation of the druggable human GPCRome. *Nat Struct Mol Biol*. 2015; 22(5): 362-369.
- Kwon, S.C., Kim, I., Song, J., Park, J. Does formaldehyde have a causal association with nasopharyngeal cancer and leukaemia?. *Ann Occup Environ Med*. 2018;30:5.
- Lee, H.J., Park, M.K., Lee, E.J., Lee, C.H. Resolvin D1 inhibits TGF- β 1-induced epithelial mesenchymal transition of A549 lung cancer cells via lipoxin A4 receptor/formyl peptide receptor 2 and GPR32. *Int J Biochem Cell Biol*. 2015;45(12):2801-7.
- Li, X., Staszewski, L., Xu, H., Durick, K., Zoller, M., and Adler, E. Human receptors for sweet and umami taste. *Proc Natl Acad Sci U S A* 2002;99:4692–4696.
- Lin, Y.C., Boone, M., Meuris, L., Lemmens, I., Van Roy, N., Soete, A., Reumers, J., Moisse, M., Plaisance, S., Drmanac, R., Chen, J., Speleman, F., Lambrechts, D., Van de Peer, Y., Tavernier, J., Callewaert, N. Genome dynamics of the human embryonic kidney 293 lineage in response to cell biology manipulations. *Nat Commun*. 2014;5:4767.
- Lu, X., Zhang, N., Meng, B., Dong, S., Hu, Y. Involvement of GPR12 in the regulation of cell proliferation and survival. *Mol Cell Biochem*. 2012 Jul;366(1-2):101-10.
- Lum, H., Qiao, J., Walter, R.J., Huang, F., Subbaiah, P.V., Kim, K.S., Holian, O. Inflammatory stress increases receptor for lysophosphatidylcholine in human microvascular endothelial cells. *Am J Physiol Heart Circ Physiol*. 2003;285: H1786–H1789.

- Luo, Y., Tanabe, E., Kitayoshi, M., Nishiguchi, Y., Fujiwara, R., Matsushima, S., Sasaki, T., Sasahira, T., Chihara, Y., Nakae, D., Fujii, K., Ohmori, H., Kuniyasu, H. Expression of MAS1 in breast cancer. *Cancer Sci.* 2015;106(9):1240-8.
- Maillet, E.L., Cui, M., Jiang, P., Mezei, M., Hecht, E., Quijada, J., Margolskee, R.F., Osman, R., Max, M. Characterization of the Binding Site of Aspartame in the Human Sweet Taste Receptor. *Chem Senses.* 2015;40(8):577-86.
- Nakajima, T., Chishima, F., Nakao, T., Hayashi, C., Kasuga, A., Shinya, K., Nakayama, T., Azuma, H., Ichikawa, G., Komatsu, A., Yamamoto, T., Kawana, K. The Expression of MAS1, an Angiotensin (1-7) Receptor, in the Eutopic Proliferative Endometria of Endometriosis Patients. *Gynecol Obstet Invest.* 2018;83(6):600-607.
- Pietz, J., Kreis, R., Rupp, A., Mayatepek, E., Rating, D., Boesch, C., Bremer, H. J. Large neutral amino acids block phenylalanine transport into brain tissue in patients with phenylketonuria. *J Clin Invest.* 1999;103(8):1169-1178.
- Pradhan, S., Shah, U.H., Mathur, A.G., Sharma, S. Aspartame: Sweetener with anti-inflammatory potential?. *J Pharmacol Pharmacother.* 2010;1(2):113–114.
- Qiao, J., Huang, F., Naikawadi, R.P., Kim, K.S., Said, T., Lum, H. Lysophosphatidylcholine impairs endothelial barrier function through the G protein-coupled receptor GPR4. *Am J Physiol Lung Cell Mol Physiol* 2006;291: L91–L101.
- Ranney, R.E., Oppermann, J.A., Muldoon, E., McMahon, F.G. Comparative metabolism of aspartame in experimental animals and humans. *J Toxicol Environ Health.* 1976;2(2):441-51.

- Recio, C., Lucy, D., Purvis, G.S.D., Iveson, P., Zeboudj, L., Iqbal, A.J., Lin, D., O'Callaghan, C., Davison, L., Griesbach, E., Russell, A.J., Wynne, G.M., Dib, L., Monaco, C., Greaves, D.R. Activation of the Immune-Metabolic Receptor GPR84 Enhances Inflammation and Phagocytosis in Macrophages. *Front Immunol.* 2018;9:1419.
- Ren, J., Zhang, Y., Cai, H., Ma, H., Zhao, D., Zhang, X., Li, Z., Wang, S., Wang, J., Liu, R., Li, Y., Qian, J., Wei, H., Niu, L., Liu, Y., Xiao, L., Ding, M., Jiang, S. Human GPR4 and the Notch signaling pathway in endothelial cell tube formation. *Mol Med Rep.* 2016;(2):1235-40.
- Rosenbaum, D.M., Rasmussen, S.G., Kobilka, B.K. The structure and function of G-protein-coupled receptors. *Nature.* 2009; 459(7245): 356–363.
- Ruiz-Ojeda, F.J., Plaza-Díaz, J., Sáez-Lara, M.J., Gil, A. Effects of Sweeteners on the Gut Microbiota: A Review of Experimental Studies and Clinical Trials. *Adv Nutr.* 2019;10:S31–S48.
- Rybakovsky, E., Valenzano, M.C., DiGuilio, K.M., Buleza, N.B., Moskalenko, D.V., Harty, R.N., Mullin, J.M. Improving Transient Transfection Efficiency in a Differentiated, Polar Epithelial Cell Layer. *J Biomol Tech.* 2019;30(2):19-24.
- Rycerz, K., Jaworska-Adamu, J.E. Effects of aspartame metabolites on astrocytes and neurons. *Folia Neuropathol.* 2013; 51(1): 10-17.
- Schmid, M., Gemperle, C., Rimann, N., Hersberger, M. Resolvin D1 Polarizes Primary Human Macrophages toward a Proresolution Phenotype through GPR32. *J Immunol.* 2016;196:3429-3437.

- Sharma, A., Amarnath, S., Thulasimani, M., Ramaswamy, S. Artificial sweeteners as a sugar substitute: Are they really safe?. *Indian J Pharmacol.* 2016; 48(3): 237–240.
- Simon, B. R., Parlee, S. D., Learman, B. S., Mori, H., Scheller, E. L., Cawthorn, W. P., Ning, X., Gallagher, K., Tyrberg, B., Assadi-Porter, F. M., Evans, C. R., MacDougald, O. A. Artificial sweeteners stimulate adipogenesis and suppress lipolysis independently of sweet taste receptors. *The Journal of biological chemistry.* 2013;288(45):32475–32489.
- Smale, S.T. Beta-galactosidase assay. *Cold Spring Harb Protoc.* 2010;5:pdb.prot5423
- Sondek, J., Bohm, A., Lambright, D.G., Hamm, H.E., Sigler P. B. Crystal structure of a G α protein $\beta\gamma$ dimer at 2.1Å resolution. *Nature* 1996; 379:369-374.
- Sun, Y.P., Oh, S.F., Uddin, J., Yang, R., Gotlinger, K., Campbell, E., Colgan, S.P., Petasis, N.A., Serhan, C.N. Resolvin D1 and Its Aspirin-triggered 17R Epimer: stereochemical assignments, anti-inflammatory properties, and enzymatic inactivation. *J Biol Chem.* 2007;282:9323-9334.
- Suzuki, M., Takaishi, S., Nagasaki, M., Onozawa, Y., Iino, I., Maeda, H., Komai, T., Oda, T. Medium-chain fatty acid-sensing receptor, GPR84, is a proinflammatory receptor. *J Biol Chem.* 2013;288(15):10684-91.
- Tirupula, K.C., Desnoyer, R., Speth, R.C., Karnik, S.S. Atypical signaling and functional desensitization response of MAS receptor to peptide ligands. *PLoS One.* 2014;9(7):e103520.

- Uhlenbrock, K., Huber, J., Ardati, A., Busch, A.E., Kostenis, E. Fluid shear stress differentially regulates gpr3, gpr6, and gpr12 expression in human umbilical vein endothelial cells. *Cell Physiol Biochem.* 2003;13(2):75-84.
- van Eyk, A.D. The effect of five artificial sweeteners on Caco-2, HT-29 and HEK-293 cells. *Drug Chem Toxicol.* 2015; 38(3): 318-327.
- Vögler, O., Barceló, J. M., Ribas, C., Escribá P. V. Membrane interactions of G proteins and other related proteins. *Biochim. Biophys. Acta* 2008; 1778:1640-1652.
- Weis, W.I., Kobilka, B.K. The Molecular Basis of G Protein-Coupled Receptor Activation. *Annu Rev Biochem.* 2018;87:897-919.
- Xu, H.E., Xiao, R.P. A new era for GPCR research: structures, biology and drug discovery. *Acta Pharmacol Sin.* 2012; 33(3): 289–290.
- Yin, Z.F., Zhang, Y.N., Liang, S.F., Zhao, S.S., Du, J., Cheng, B.B. Mycoplasma contamination-mediated attenuation of plasmid DNA transfection efficiency is augmented via L-arginine deprivation in HEK-293 cells. *J Zhejiang Univ Sci B.* 2019;20(12):1021–1026.
- Yu, M., Cui, R., Huang, Y., Luo, Y., Qin, S., Zhong, M. Increased proton-sensing receptor GPR4 signalling promotes colorectal cancer progression by activating the hippo pathway. *EBioMedicine.* 2019;48:264–276.

Supplementary Data

Table 1: GPCR screen receptor number and the corresponding official GPCR orphan receptor name along with RLU value and P-Value determined using R Studio, where N=3.

| Receptor Number | GPCR Name | RLU Set A | RLU Set C | RLU Set D | RLU Set E | P-Value Set A | P-Value Set C | P-Value Set D | P-Value Set E |
|------------------------|------------------|------------------|------------------|------------------|------------------|----------------------|----------------------|----------------------|----------------------|
| R1 | <i>CMKOR1</i> | 1611 | 2048 | 4437 | 538 | 0.257 | 0.700 | 0.975 | 0.600 |
| R10 | <i>GPR133</i> | 3381 | 1594 | 5408 | 1821 | 0.567 | 0.349 | 0.159 | 0.255 |
| R11 | <i>GPR141</i> | 21808 | 19969 | 11400 | 6817 | 0.711 | 0.071 | 1.000 | 0.564 |
| R12 | <i>GPR142</i> | 4811 | 1875 | 1056 | 1289 | 0.455 | 0.239 | 0.130 | 0.209 |
| R13 | <i>GPR143</i> | 5059 | 2170 | 1251 | 1208 | 0.470 | 0.136 | 0.168 | 0.102 |
| R14 | <i>GPR144</i> | 3782 | 2707 | 1947 | 1871 | 0.160 | 0.161 | 0.152 | 0.200 |
| R15 | <i>GPR146</i> | 2106 | 3286 | 3688 | 2387 | 0.387 | 0.750 | 0.100 | 1.000 |
| R16 | <i>GPR148</i> | 3711 | 2678 | 1145 | 1816 | 0.152 | 0.676 | 0.805 | 0.575 |
| R17 | <i>GPR149</i> | 1207 | 1229 | 1136 | 1225 | 0.348 | 0.100 | 0.385 | 0.418 |
| R18 | <i>GPR15</i> | 2793 | 4600 | 5525 | 2463 | 0.529 | 0.716 | 0.502 | 0.700 |
| R19 | <i>GPR150</i> | 6367 | 15938 | 1113 | 1201 | 0.605 | 0.896 | 1.000 | 0.400 |
| R2 | <i>GPER</i> | 2317 | 2031 | 3127 | 3550 | 0.100 | 0.046 | 0.919 | 0.400 |
| R20 | <i>GPR151</i> | 2145 | 3905 | 1094 | 940 | 0.547 | 0.274 | 1.000 | 0.027 |
| R21 | <i>GPR153</i> | 10545 | 10194 | 1638 | 1249 | 0.060 | 0.700 | 0.700 | 0.013 |
| R22 | <i>GPR156</i> | 10324 | 32104 | 21170 | 13662 | 0.544 | 0.186 | 1.000 | 0.700 |
| R23 | <i>GPR160</i> | 4716 | 11043 | 13363 | 3633 | 0.313 | 0.399 | 0.660 | 0.139 |
| R24 | <i>GPR161</i> | 15461 | 37709 | 44635 | 19039 | 0.236 | 0.703 | 0.700 | 0.700 |
| R3 | <i>GPR101</i> | 73705 | 59660 | 47502 | 615 | 0.065 | 0.696 | 0.971 | 0.100 |
| R4 | <i>GPR110</i> | 3506 | 2946 | 1665 | 738 | 1.000 | 0.682 | 0.939 | 0.000 |
| R5 | <i>GPR113</i> | 6100 | 6108 | 2502 | 1025 | 0.881 | 0.957 | 0.100 | 0.006 |
| R6 | <i>GPR116</i> | 3994 | 6426 | 1448 | 1269 | 0.680 | 0.645 | 0.398 | 0.183 |
| R7 | <i>GPR12</i> | 66986 | 102385 | 104837 | 37421 | 0.180 | 0.735 | 0.902 | 0.020 |
| R8 | <i>GPR123</i> | 9373 | 7650 | 3653 | 1055 | 0.569 | 0.463 | 0.126 | 0.002 |
| R9 | <i>GPR132</i> | 18698 | 18483 | 22373 | 716 | 0.492 | 0.607 | 0.400 | 0.400 |
| R25 | <i>GPR162</i> | 1153 | 3157 | 1076 | 876 | 0.120 | 0.400 | 0.631 | 0.938 |
| R26 | <i>GPR17</i> | 23926 | 112745 | 2746 | 252287 | 0.636 | 0.353 | 0.674 | 0.520 |
| R27 | <i>GPR171</i> | 2740 | 3282 | 684 | 2032 | 0.345 | 0.700 | 0.143 | 0.536 |
| R28 | <i>GPR173</i> | 11732 | 48591 | 476 | 10124 | 0.423 | 0.100 | 0.100 | 0.022 |
| R29 | <i>GPR182</i> | 345330 | 557666 | 870 | 55255 | 0.418 | 0.895 | 0.971 | 0.138 |
| R30 | <i>GPR19</i> | 19858 | 51242 | 616 | 5331 | 0.357 | 0.100 | 0.729 | 0.792 |
| R31 | <i>GPR20</i> | 2721 | 131753 | 1758 | 1558 | 0.171 | 0.917 | 0.238 | 0.216 |
| R32 | <i>GPR23</i> | 139106 | 149469 | 801 | 7849 | 0.958 | 0.816 | 0.532 | 0.873 |
| R33 | <i>GPR25</i> | 21270 | 21666 | 1665 | 1700 | 0.551 | 0.176 | 0.687 | 0.245 |
| R34 | <i>GPR26</i> | 15831 | 13624 | 5042 | 5261 | 0.417 | 0.100 | 0.695 | 0.946 |
| R35 | <i>GPR27</i> | 1804 | 2020 | 973 | 1394 | 0.695 | 0.700 | 0.939 | 0.597 |
| R36 | <i>GPR31</i> | 5919 | 7994 | 1311 | 1916 | 0.388 | 0.068 | 0.310 | 0.882 |
| R37 | <i>GPR32</i> | 35834 | 86084 | 13061 | 18734 | 0.042 | 0.113 | 0.028 | 0.026 |
| R38 | <i>GPR35</i> | 29791 | 79231 | 26756 | 47997 | 0.602 | 0.370 | 0.930 | 0.053 |
| R39 | <i>GPR37</i> | 242003 | 426292 | 767727 | 445223 | 0.463 | 0.251 | 0.771 | 0.368 |
| R40 | <i>GPR37L1</i> | 4942 | 4640 | 3253 | 6305 | 1.000 | 0.200 | 0.479 | 0.304 |

| | | | | | | | | | |
|-----|----------------|--------|--------|---------|--------|-------|-------|-------|-------|
| R41 | <i>GPR39</i> | 4842 | 5783 | 13709 | 4085 | 0.278 | 0.412 | 0.700 | 0.554 |
| R42 | <i>GPR4</i> | 27584 | 50401 | 368470 | 67905 | 0.566 | 0.025 | 0.100 | 0.418 |
| R43 | <i>GPR45</i> | 29535 | 70623 | 10165 | 5937 | 0.417 | 1.000 | 0.105 | 0.045 |
| R44 | <i>GPR52</i> | 14817 | 38674 | 17342 | 11338 | 0.194 | 0.231 | 0.021 | 0.962 |
| R45 | <i>GPR55</i> | 3185 | 12278 | 6614 | 5216 | 0.723 | 0.380 | 0.236 | 0.197 |
| R46 | <i>GPR6</i> | 135265 | 599485 | 560770 | 706526 | 0.415 | 0.156 | 0.011 | 0.215 |
| R47 | <i>GPR61</i> | 8914 | 10599 | 9952 | 9137 | 0.700 | 0.663 | 0.077 | 0.063 |
| R48 | <i>GPR62</i> | 4009 | 3991 | 2413 | 928 | 0.019 | 0.400 | 0.334 | 0.200 |
| R49 | <i>GPR63</i> | 1080 | 2736 | 3956 | 1925 | 0.700 | 0.100 | 0.249 | 0.100 |
| R50 | <i>GPR64</i> | 1736 | 3433 | 13161 | 3275 | 0.411 | 0.211 | 0.341 | 0.136 |
| R51 | <i>GPR78</i> | 16497 | 15902 | 3875 | 4446 | 0.190 | 0.700 | 0.700 | 0.001 |
| R52 | <i>GPR83</i> | 3833 | 4377 | 1866 | 1522 | 0.875 | 0.044 | 0.100 | 0.619 |
| R53 | <i>GPR84</i> | 28553 | 77433 | 54610 | 24073 | 0.019 | 0.356 | 0.264 | 0.152 |
| R54 | <i>GPR85</i> | 20581 | 48997 | 30829 | 25688 | 0.523 | 0.168 | 0.459 | 0.534 |
| R55 | <i>GPR87</i> | 47626 | 189897 | 1110117 | 478583 | 0.095 | 0.662 | 0.700 | 0.100 |
| R56 | <i>GPR88</i> | 2450 | 4158 | 2262 | 1870 | 0.850 | 0.700 | 0.121 | 0.037 |
| R57 | <i>GPR54</i> | 14141 | 9137 | 1575 | 949 | 0.375 | 0.745 | 0.811 | 0.373 |
| R58 | <i>MAS1</i> | 104278 | 133107 | 475363 | 277156 | 0.401 | 1.000 | 0.045 | 0.320 |
| R59 | <i>MAS1L</i> | 4046 | 14997 | 3128 | 4495 | 0.738 | 0.898 | 0.100 | 0.065 |
| R60 | <i>MRGPRD</i> | 3335 | 4950 | 1370 | 1050 | 0.253 | 0.262 | 0.349 | 0.100 |
| R61 | <i>MRGPRF</i> | 5241 | 53308 | 25268 | 22010 | 0.665 | 0.697 | 0.088 | 0.084 |
| R62 | <i>MRGPRG</i> | 1009 | 3226 | 4731 | 2252 | 0.679 | 0.256 | 0.396 | 0.198 |
| R63 | <i>MRGPRX1</i> | 1386 | 2784 | 4758 | 2418 | 0.632 | 0.121 | 0.249 | 0.184 |
| R64 | <i>MRGPRX2</i> | 15950 | 36000 | 47773 | 72312 | 0.308 | 0.556 | 0.700 | 0.349 |
| R65 | <i>MRGPRX4</i> | 3438 | 6254 | 3177 | 5543 | 0.694 | 0.383 | 0.200 | 0.062 |
| R66 | <i>OPN3</i> | 934 | 1672 | 4664 | 621 | 0.201 | 0.044 | 0.864 | 0.230 |
| R67 | <i>OPN5</i> | 79040 | 103466 | 75046 | 223743 | 0.169 | 0.430 | 0.449 | 0.787 |
| R68 | <i>PK2</i> | 3858 | 2600 | 981 | 2525 | 0.182 | 0.100 | 0.853 | 0.505 |
| R69 | <i>PRP</i> | 8270 | 13730 | 5786 | 11503 | 0.088 | 0.993 | 0.195 | 0.191 |
| R70 | <i>TAAR5</i> | 1514 | 1481 | 1340 | 3659 | 0.923 | 0.115 | 0.813 | 0.724 |
| R71 | <i>TAAR6</i> | 18376 | 17312 | 24607 | 11415 | 0.700 | 0.990 | 1.000 | 0.652 |
| R72 | <i>TAAR9</i> | 2872 | 4380 | 1451 | 1634 | 0.659 | 0.855 | 0.572 | 0.240 |

Table 2: GPCR receptor and the corresponding Rourke lab stock number, concentration (ng/ μ L) as well as the A260/A280 ratio. Prepped using the Promega Pure Yield Miniprep and concentrations were found using the Nanodrop software.

| Receptor | Rourke Stock # | Concentration (ng/μL) | A260 | A280 | A260/A280 |
|-----------------|-----------------------|---|-------------|-------------|------------------|
| <i>GPR151</i> | 21 | 636.03 | 12.72 | 6.57 | 1.94 |
| <i>GPR113</i> | 22 | 659.47 | 13.19 | 6.75 | 1.95 |
| <i>GPR116</i> | 23 | 178.32 | 3.57 | 1.90 | 1.88 |
| <i>GPR12</i> | 24 | 414.51 | 8.29 | 4.53 | 1.83 |
| <i>GPR123</i> | 25 | 449.62 | 8.99 | 4.92 | 1.83 |
| <i>GPR132</i> | 26 | 499.29 | 9.99 | 5.55 | 1.80 |
| <i>GPR133</i> | 27 | 582.04 | 11.64 | 6.53 | 1.78 |
| <i>GPR141</i> | 28 | 697.80 | 13.96 | 7.23 | 1.93 |
| <i>GPR142</i> | 29 | 516.84 | 10.34 | 5.74 | 1.80 |
| <i>GPR26</i> | 53 | 534.20 | 10.68 | 5.96 | 1.79 |
| <i>GPR27</i> | 54 | 450.37 | 9.01 | 5.02 | 1.80 |
| <i>GPR3</i> | 55 | 522.77 | 10.46 | 5.89 | 1.78 |
| <i>GPR31</i> | 56 | 565.52 | 11.31 | 6.44 | 1.76 |
| <i>GPR32</i> | 57 | 189.74 | 3.80 | 2.04 | 1.86 |
| <i>GPR35</i> | 58 | 299.66 | 5.99 | 3.22 | 1.86 |
| <i>GPR37</i> | 59 | 433.11 | 8.66 | 4.85 | 1.79 |
| <i>GPR37L1</i> | 60 | 458.61 | 9.17 | 5.12 | 1.79 |
| <i>GPR39</i> | 61 | 502.10 | 10.04 | 5.61 | 1.79 |
| <i>GPR4</i> | 62 | 437.96 | 8.76 | 4.86 | 1.80 |
| <i>GPR45</i> | 63 | 289.54 | 5.79 | 3.16 | 1.83 |
| <i>GPR52</i> | 64 | 74.56 | 1.49 | 0.79 | 1.89 |
| <i>GPR55</i> | 65 | 170.28 | 3.41 | 1.81 | 1.88 |
| <i>GPR56</i> | 66 | 529.20 | 10.58 | 5.80 | 1.82 |
| <i>GPR6</i> | 67 | 577.54 | 11.55 | 6.40 | 1.81 |
| <i>GPR61</i> | 68 | 576.38 | 11.53 | 6.41 | 1.80 |
| <i>GPR62</i> | 69 | 643.91 | 12.88 | 6.82 | 1.89 |
| <i>GPR63</i> | 70 | 117.62 | 2.35 | 1.25 | 1.88 |
| <i>GPR64</i> | 71 | 560.02 | 11.20 | 6.30 | 1.78 |
| <i>GPR78</i> | 72 | 545.30 | 10.91 | 6.04 | 1.81 |
| <i>GPR84</i> | 73 | 645.53 | 12.91 | 6.93 | 1.86 |
| <i>GPR85</i> | 74 | 572.51 | 11.45 | 6.40 | 1.79 |
| <i>GPR87</i> | 75 | 467.48 | 9.35 | 5.14 | 1.82 |
| <i>GPR52</i> | 64 | 81.93 | 1.64 | 0.88 | 1.87 |
| <i>GPR17</i> | 35 | 23.46 | 0.47 | 0.26 | 1.78 |

Table 3: PEI transfection efficiency calculated by GFP cells counted at 10X magnification using an EVOS microscope versus the total number of cells counted at 10X magnification.

| PEI/Well (μL) | GFP Cells | Total Cells | % Efficiency |
|-------------------------------------|------------------|--------------------|---------------------|
| 0.05 | 0 | N/A | N/A |
| 0.01 | 0 | N/A | N/A |
| 0.2 | 68.3 | 1188 | 5.75 |
| 0.3 | 272.7 | 1107.7 | 24.62 |
| 0.4 | 184 | 1198.3 | 15.35 |

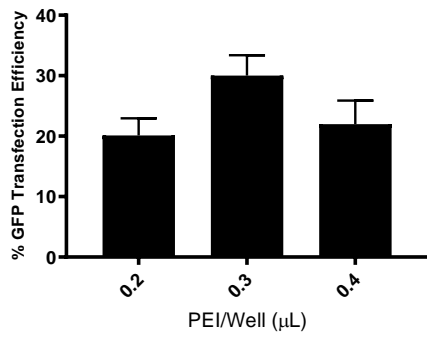
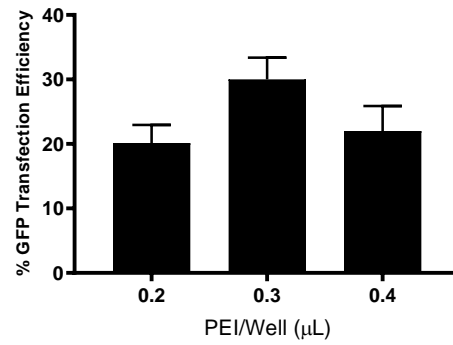
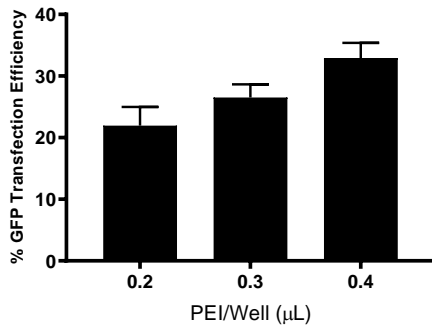
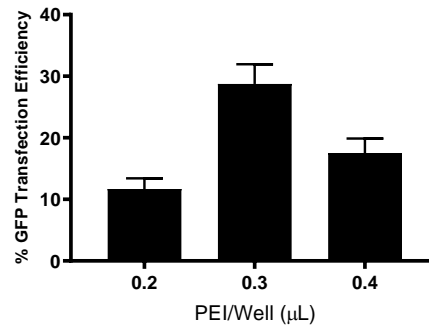
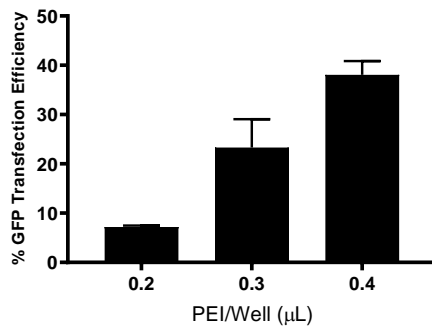
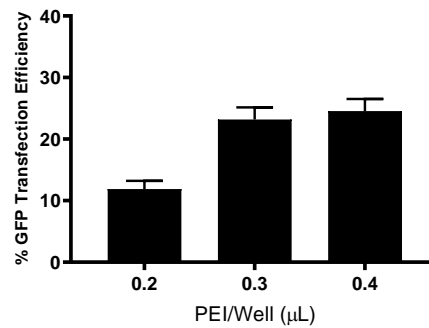
A**B****C****D****E****F**

Figure 20: The transfection efficiency of GFP using various concentrations of PEI in each cell well at various plated cell per well amounts; 5000 (**A**), 10 000 (**B**), 15 000 (**C**), 20 000 (**D**), 25 000 (**E**) and 30 000 (**F**) cells per well.